NGU Report 2008.003

Feasibility study of integrated electromagnetic, gravimetric, aeromagnetic and seismic sub-basalt exploration techniques.

Geological Survey of Norway
N-7441 Trondheim, Norway
Tel.: 47 73 90 40 00
Telefax 47 73 92 16 20

REPORT

Report no.: 2008.003 | ISSN 0800-3416 | Grading: Confidential to January 2013

Title:
Feasibility study of integrated electromagnetic, gravimetric, aeromagnetic and seismic sub-basalt exploration techniques.

Authors:
Stein Fanavoll, Reynir Fjalar Reynisson,
Grunde Waag, Peter Walker & Jörg Ebbing.

Client:
Force Group
NPD

County:

Commune:

Map-sheet name (M=1:250.000)

Map-sheet no. and -name (M=1:50.000)

Deposit name and grid-reference:

Number of pages: 66
Map enclosures:

Price (NOK):

Fieldwork carried out:

Date of report:

Project no.:
3209.00

Person responsible:

Summary:

The objective of this study was to investigate methods to resolve the problem of mapping basalts and basement in a continental margin setting. It is well known that basalts may trap considerable amounts of hydrocarbons accumulated in sediments below the basalts. A 3D model of the Møre margin offshore Norway was constructed by forward modelling employing the gravity and magnetic fields. Numerous independent data were used to diminish the nonuniqueness of the method. The resulting model consists of several horizons that divide the main geological bodies in the study area. In addition, two horizons are based on reflection seismic interpretation only. Based on gravity/magnetic modelling and seismic interpretation, a layer model was constructed in RMS. Three different models were run through the emgs 3D modelling software, varying thickness as well as resistivity of the volcanics and basement. The presence of volcanics were clearly detected by the SBL method. However, there is an upper threshold value of the thickness/resistivity product, where the SBL method becomes insensitive to variations in either thickness of the layer, or the resistivity. Below this threshold value variations in thickness and resistivity will influence the results. Hydrocarbon reservoirs may be identified as small anomalies, but only when the background model is known, and only for large reservoirs. 2D inversion of three synthetic MMT models was done in this feasibility study. One model included only a simple basalt structure. The MMT response was not sensitive to this structure, because the contrast to the background resistivity was too small. In the second model the basement was added, in addition to the basalt. The basement boundary could be seen clearly from the inversion results and in the individual receiver responses. Finally, an increase in the basalt thickness was tested. The MMT results were now sensitive to the basalt layer, but failed to resolve the sediments between the basalts and the basement where the thickness is at its thinnest (1500 m).

Keywords: Geophysics	Gravity	Magnetics
Continental Shelf	Seismic	Electromagnetics
	Sub-basalt	Industrial report

CONTENTS

FIGURES

TABLES

1. INTRODUCTION

1.1 Background

Large areas of passive ocean margins are covered by basalts that may conceal enormous reserves of hydrocarbons. For example, the northeast Atlantic margin is relatively unexplored and holds the promise of large hydrocarbon accumulations. However, in most of this area, the Mesozoic and Palaeozoic sediments that are of interest for hydrocarbon exploration are covered by Cenozoic flood basalts. The crust on the Norwegian margin has been strongly affected by the volcanism, in particular in the outer part of the commercially exploitable Møre and Vøring Basins, where extrusive and intrusive rocks form an important part of the basin fill.

Standard seismic acquisition and processing fails to deliver interpretable images of the sub-basalt sequences. One of the keys to unlocking the huge potential of the margin is to characterize the basalt and find better methods to image beneath it. A useful technique in the presence of seismically problematical lithologies is modelling of potential field and electromagnetic data. Gravity modelling can significantly improve the seismic interpretation and may especially help with understanding the structural interpretation in areas obscured by volcanics. The combined use of electromagnetic, gravity and magnetic data add further constraints to the interpretations.

1.2 Objectives

- Construct model of sub-basalt structures on the Møre Margin from potential field, seismic and well log data (incl. reprocessed NPD lines from the MB-92 survey)
- Attribute electric resistivity data to the model
- Simulate the electromagnetic response along line GMNR-94-102 for the given geometry over the most likely 3D geo-model.
- Select optimal frequencies and transmitter waveform for a following acquisition if the method is applicable.

1.3 Construction of 3D crustal model

The Interactive Gravity and Magnetic Application System (IGMAS) was used to build a 3D structural model based on potential field data (gravity and magnetics). The modelled area encompasses the Møre margin from the onshore to the oceanic domain (Figure 1.1). The model consists of 21 cross-sections with a spacing of 20 km. Each cross-section is made up of several geometrical bodies with varying physical properties (density, susceptibility, remnant magnetization and P-wave velocity) that represent different geological units. The model was geometrically constrained by seismic data (reflection and refraction) and physical properties were based on well data, seismic velocity-depth studies, and onshore analogues. Differences

between the observed and predicted magnetic and gravity fields were then used as the basis for refining the model geometries.

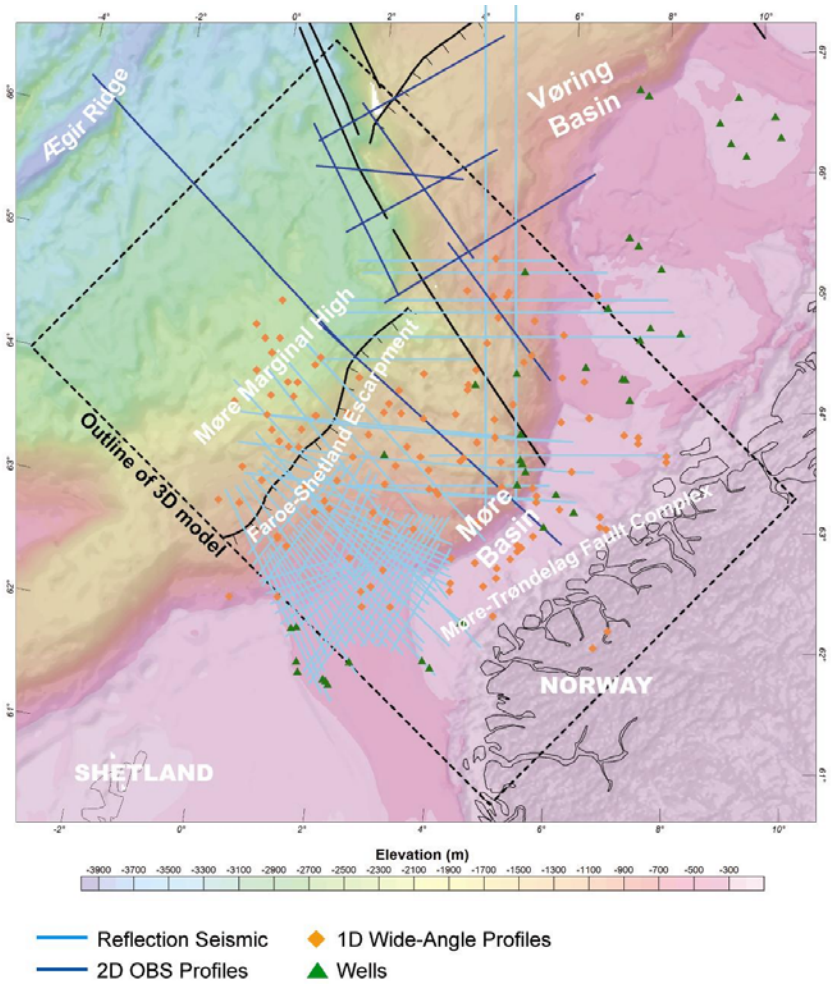

Figure 1.1 *Outline of the 3D model and location of data sets used to constrain the gravity and magnetic modelling.*

1.4 EM Feasibility Modelling

EM feasibility modelling may comprise SBL 3D or MMT (Marine Magneto-Tellurics). For a setting involving other high resistive layer, such as basalts, a joint CSEM and MMT study is usually recommended. The modelling will be carried out along line GMNR-94-102 (Figure 1.2) that will be reprocessed especially for the proposed IODP well on the Møre Margin.

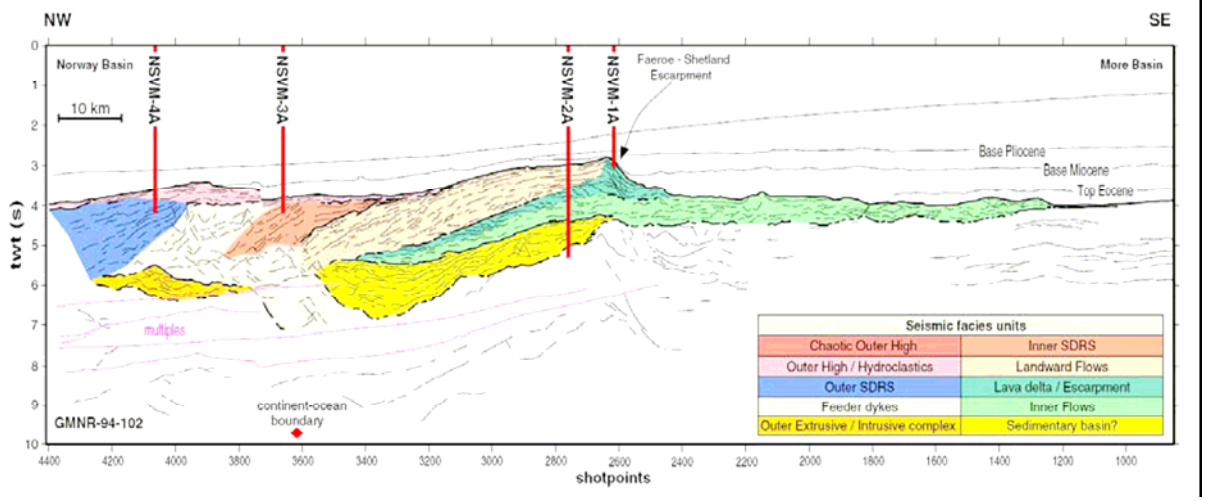

Figure 1.2 Seismic interpretation along the seismic GMNR-94-102 line (Planke & Alvestad 1999).

1.5 Work plan

- Building of most likely geo-model based on potential field data
- Conversion of geo model into resistivity model
- Run simulation for the model for
- one set of receiver and transmitter coordinates, a maximum of three receiver-transmitter lines
- for a maximum of 5 frequencies in 3D and 20 frequencies in 1D simulations
- Post process the modelled data
- Test sensitivity to varying resistivity values
- Take noise floor into account
- Create map and summary for both standard processed and up-down separated data where applicable
- Assess the feasibility of EM methods (Sea Bed Logging [SBL] and Marine Magneto-Tellurics [MMT]) for the sub-basalt imaging
- Present result from the feasibility study

2. 3D GEOLOGIC MODELLING

Reynir Fjalar Reynisson & Jörg Ebbing, NGU/NTNU

2.1 Introduction

The Møre volcanic margin (Figure 2.1) is a part of the mid-Norwegian margin, one of the world's most extensively studied continental margins. Volcanic margins are considered an end-member of rifted margins and generally characterized by transient, voluminous basaltic volcanism that impedes imaging of deeper structures. Modern aeromagnetic and gravity compilations from the Geological Survey of Norway provide a tool to address some of the questions remaining on the Møre margin. The key questions relate to the maximum extension and nature of the continental crust beneath the volcanic material emplaced during break-up in Early Tertiary time. To address these problems a 3D density and magnetic model on the Møre margin was constructed. Differences between the observed and predicted magnetic and gravity fields were used as the basis for refining the model geometries that were based on numerous additional datasets. The model provides new and relevant constrains about the maximum extent of the true continental basement, sub-basalt geometry, the nature of the rift and proto-ridge structures and the distribution of lower crustal bodies expected along this volcanic frontier area.

2.2 Data

The gravity data used in this study is based on a compilation by Skilbrei et al. (2000). The compilation consists of marine gravity data from the Geological Survey of Norway, the Norwegian Mapping Authority, the Norwegian Petroleum Directorate, Norwegian and foreign universities, and commercial companies. Gravity data derived from satellite altimetry were used in the deep-water areas of the Norwegian-Greenland Sea (Andersen & Knudsen 1998, Laxon & McAdoo 1994). The International Standardization Net 1971 (IGSN 71) and the Gravity Formula 1980 for normal gravity were used to level the different surveys. From the compiled free-air dataset a Bouguer reduction at sea was carried out. The reduction was based on bathymetry data from Dehls et al. (2000) and a density of 2200 kg/m^3 (Figure 2.2).

The magnetic data compilation is from Olesen et al. (1997) that includes mostly total-intensity airborne measurements and some additional shipborne measurements. Flight altitudes, flying directions, and line-spacings of the aeromagnetic surveys vary widely. A reference to the Definite Geomagnetic Reference Field (DGRF 1965.0) was used to produce the total magnetic field anomaly grid with 1x1 km cells (Figure 2.3).

In addition to the gravity and magnetic data numerous datasets were used to further constrain the model (Figure 2.4). Depth converted base Tertiary and base Cretaceous horizons from Shell provided valuable geometrical constraints. Published OBS profiles (Breivik et al. 2006, Raum et al. 2002, Raum et al. 2006) provided guide to the deeper structures. 1D velocity profiles based on ESP and sonobuoy experiments in the study area were used to help to

identify the basement (Eldholm & Mutter 1986, Ólafsson et al. 1992, Planke et al. 1991). Seismic reflection lines provided by Shell/Fugro (MNR-05), the GMNR94-102 line, and reprocessed lines from NPD (MB-92) were used to interpret the general structure, compare to the model and adjust if necessary. The top of the basalts, both extrusives and intrusives, were mapped on Shell's extensive seismic database and depth converted to provide information on the spatial distribution of volcanics in the area. In addition, the Moho compilation by Kinck et al. (1993) and its modifications by Olesen et al. (2002) were used to constrain the model in the coastal area.

The petrophysical properties used in the model (Table 2.1) are based on various sources. For the sediments 23 composite logs from exploration wells were studied to acquire appropriate densities and the magnetic properties are based on extensive study by Mørk et al. (2002). Properties for the basement, lower-crust and mantle are based on previous model studies (Ebbing et al. 2006, Fernàndez et al. 2005, Fernàndez et al. 2004, Olesen et al. 2002). The Deep Sea Drilling Project (DSDP) and Ocean Drilling Program (ODP) in the Vøring area (Eldholm et al. 1987, Kent & Opdyke 1978, Planke & Alvestad 1999, Planke et al. 1999, Planke & Eldholm 1994) in addition to measurements from the Faroe Islands (Abrahamsen et al. 1984, Abrahamsen & Waagstein 2006, Balling et al. 1984, Saxov & Abrahamsen 1964, Schoenharting & Abrahamsen 1984) and Iceland (Franzson et al. 2001, Friðleifsson 1982, Friðleifsson et al. 1982, Helgason 1982, Jónsson & Stefánsson 1982, Kristjansson & Helgason 1988, Pálsson et al. 1984) provided density and magnetic properties for the igneous bodies of the model.

Table 2.1 Overview of physical properties used in the model (see references in text).

	Density (g/cm^3)	Susceptibility (10^{-5} SI)	Köningsberg ratio
Water	2.20		
Cenozoic	2.10	200	0.1
Cretaceous	2.40	30	0.1
Pre-Cretaceous	2.55	30	0.1
Continental Basement	2.70	2000	1
Continental Lower Crust	2.85	2000	1
Oceanic Basement	2.80	3000	2
Oceanic Lower Crust	2.90	3000	2
Sills	0.05	1000	1
LCB	3.10	3000	2
Mantle-1	3.27		
Mantle-2	3.28		
Mantle-3	3.30		
Mantle-4	3.31		
ref-1 (0-12 km)	2.67		
ref-2 (12-30 km)	2.75		
ref-3 (30-200 km)	3.31		

2.3 Modelling Approach

The Interactive Gravity and Magnetic Application System (IGMAS; http://www.gravity.uni-kiel.de/igmas) was used for the 3D forward modelling. The system calculates the potential field effect of the model by triangulation between modelling planes (Götze & Lahmeyer 1988). The model consists of 21 cross-sections with a spacing of 20 km (Figure 2.4). Each cross-section consists of several geometrical bodies with varying physical properties (Figure 2.5a-c and Table 2.1).

The main assumptions in the modelling process were that each geometrical body is representative of a regional geological structure, each body has a constant density and magnetic properties, and the Curie isotherm coincides with the Moho meaning the mantle does not contribute to the magnetic signal. The mantle was the only body that was allowed to vary laterally to represent higher thermal gradient in the oceanic domain than in the continental domain (c.f. Breivik et al. 1999; Olesen et al. 2002, Fernàndez et al. 2004).

To diminish the effect of the seabed in the modelling process an offshore Bouguer reduction was carried out on the free air gravity data set. Bouguer anomalies only express relative gravity and therefore density contrasts of all lateral inhomogeneities cause the modelled field. In order to model the absolute density and avoid edge effects a reference density model was introduced into the model. The reference model provides opportunities to compare the density model with petrologic and seismic velocity models. It was divided into three layers with densities based on global scale velocity and density distribution in the Lithosphere (Dziewonski & Anderson 1981).

Both the gravity and magnetic data were used without any filtering to ensure as little information in the datasets as possible were missing from the interpretation.
Separation of deep sources from shallow with wavelength filtering (e.g. high pass filtering) is problematic because the wavenumber spectra (wavelength = 1/wavenumber) of most geological features are broadband. This means that spectra of features at different depths overlap and consequently the features cannot be separated completely by filtering (Telford et at. 1990). In order to incorporate the whole spectra in the modelling process the model starts at 200 km depth and extends laterally well beyond the study area.

Like a gravity anomaly, the shape of a magnetic anomaly depends on the shape of the causative body. Unlike a gravity anomaly, a magnetic anomaly also depends on the inclination and declination of the body's magnetization, the inclination and declination of the local earth's magnetic field, and the orientation of the body with respect to magnetic north. To simplify the anomaly shape an operation known as reduction to the pole is often used. This operation transforms the observed magnetic anomaly into the anomaly that would have been measured if the magnetization and ambient field were both vertical or as if the measurements were made at the magnetic pole. It was not needed to introduce this operation to the magnetic data in this study because the modelling software accounts for the declination and inclination

of both the ambient field and the magnetized body and also because of the already high inclination of the magnetic field in the study area.

The basaltic thickness and sub-basaltic basement structure (and consequently sedimentary thickness) is of a major exploration interest. The model presented in this study predicts these features but faced by the fundamental problem of potential fields, the ambiguity, and the fact that this is a large scale regional model the results can only be viewed as an indication. For example a decrease in density from 2.8 to 2.6 g/cm^3 in the oceanic basement would result in an increased thickness estimate of about 1000 m. Different physical parameters in sub-basaltic bodies would also result in different geometrical layouts.

Because of the ambiguity of potential field interpretation the model presented here is one of several possible models, which has been developed by an iterative, interactive procedure, trying to satisfy as much constraining data as presently available. The greatest uncertainty is on the outer margin where only poor or no seismic control exists. Nevertheless, the sub-basaltic structure on the marginal high is supported by reflections observed on the GMNR94-102 and MB-92 lines that were not employed in the construction of the initial model. Figure 2.6 presents a comparison of modelled cross-section to the GMNR94-102 line. It is apparent that the model lacks the detail of the seismic lines but on the other hand it gives an indication of structures that are hardly or not at all visible on the seismic.

The accuracy of the model also depends on the quality of the data. The gravity and magnetic compilations used in this study did not include all existing surveys in the area as they are non-released industrial data. Several gravity surveys are missing from the compilation and two high quality magnetic surveys (NB-07 and MBAM-97) are also missing from this study. A more dense dataset could be used to construct a more localized model that would decrease the geometrical uncertainty of the modelled bodies.

2.4 Results

From the 3D density and magnetic model several surfaces were mapped. The maps produced for this study were the seabed, top basalt, base basalt, base Tertiary, base Cretaceous and top basement. The base basalt and base Tertiary horizons were combined in one (Figures 2.7a and b). From seismic reflection interpretation top saucer shaped sills and top sill complexes were also mapped.

The top basalt horizon was well constrained by seismic reflection data and has a high confidence level. The top upper sills were easily recognized in the basin on seismic data, but oceanward of the escarpment they are very difficult to identify both on seismic and potential field data. The top lower sills could be mapped with medium confidence in the basin but are untraceable beyond the escarpment. Of the base igneous bodies only the base basalt was modelled as this horizon slightly affected the potential fields. On a regional scale the confidence level of this horizon is acceptable but as the choice of parameters affects the

thickness estimate in the scale of 100s of meters the confidence level is low on a local scale. It was not possible to produce the base upper and lower sills horizons from the model. The base Tertiary was well constrained by seismic reflection data and has a high confidence level throughout the study area. For most of the area the base Cretaceous was also well constrained but in the deeper parts of the basin and below sills and especially on the marginal high the confidence reduces dramatically. It is impossible to distinguish between Cretaceous and Pre-Cretaceous sediments in the basaltic areas. Only the low density and magnetic properties of sediments give an indication of their presence below the basalts and hence the top basement structure. Even on the more landward part of the margin the top basement can not be easily determined from seismic and its modelled structure relies to a high degree on the potential field response.

2.5 Summary

A 3D model of the Møre margin offshore Norway was constructed by forward modelling employing the gravity and magnetic fields. Numerous independent data were used to diminish the nonuniqueness of the method. The resulting model consists of several horizons that divide the main geological bodies in the study area. In addition two horizons are based on reflection seismic interpretation only. The horizons presented in this study are:

- Seabed
- Top basalt
- Base basalt / base Tertiary
- Base Cretaceous
- Top Basement
- Top saucer shaped sills (seismic interpretation only)
- Top sill complexes (seismic interpretation only)

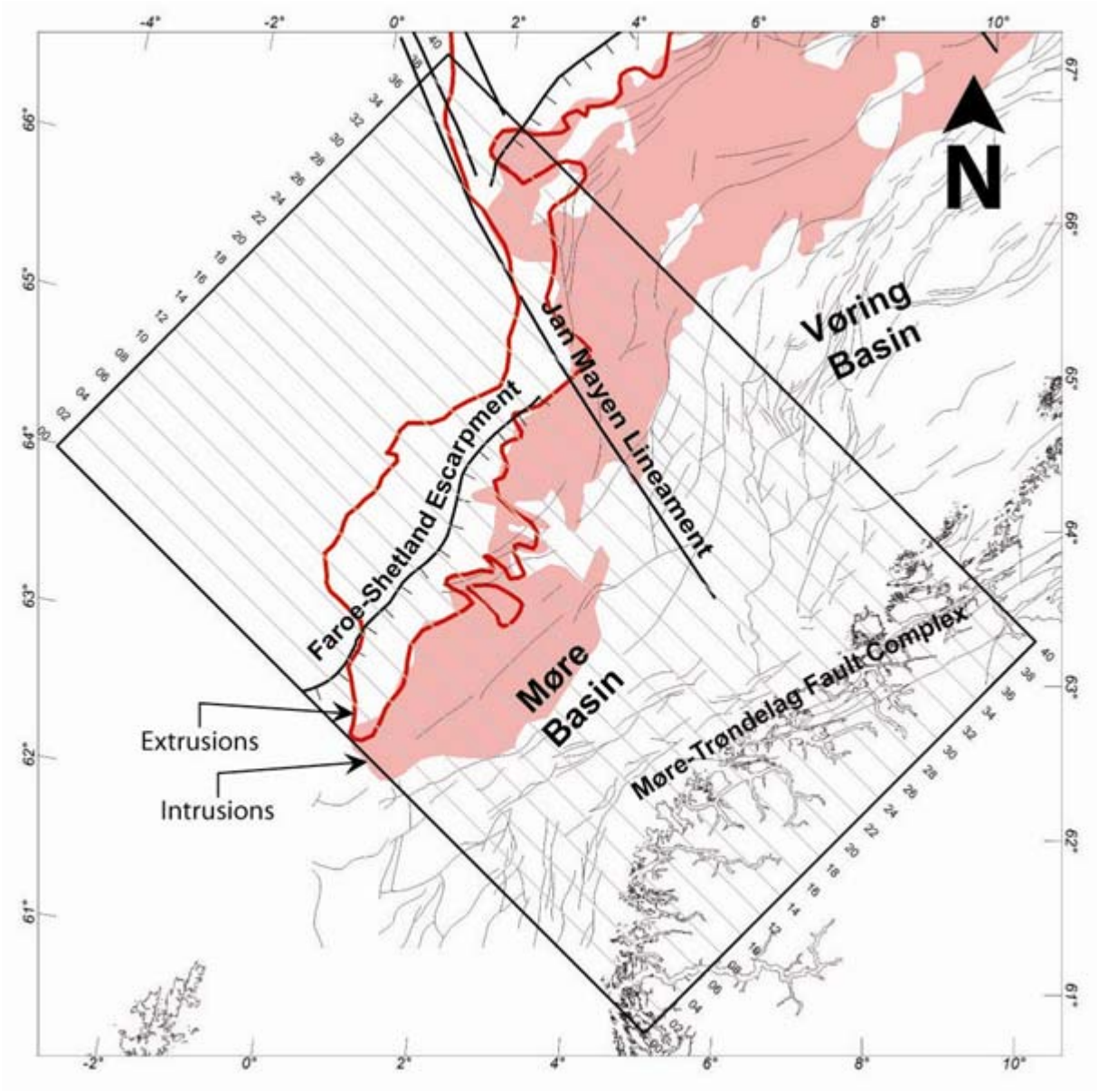

Figure 2.1 *The outlined area indicates the study area that is 400 km wide and 600 km long. Structural elements from Blystad et al. (1995) and distribution of volcanics from Planke et al. (2005).*

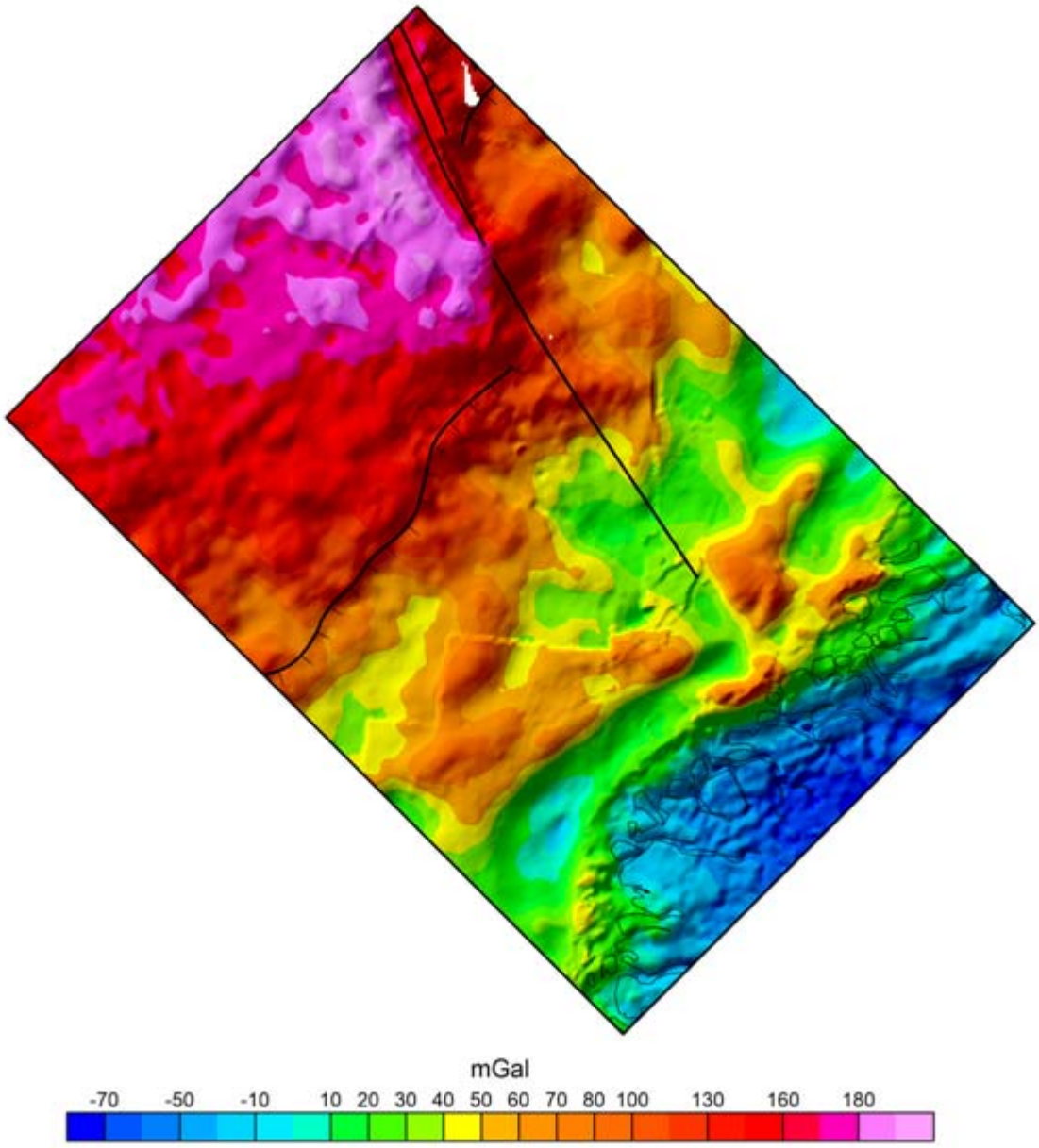

Figure 2.2 Bouguer gravity anomaly map. See location of study area on Figure 2.1.

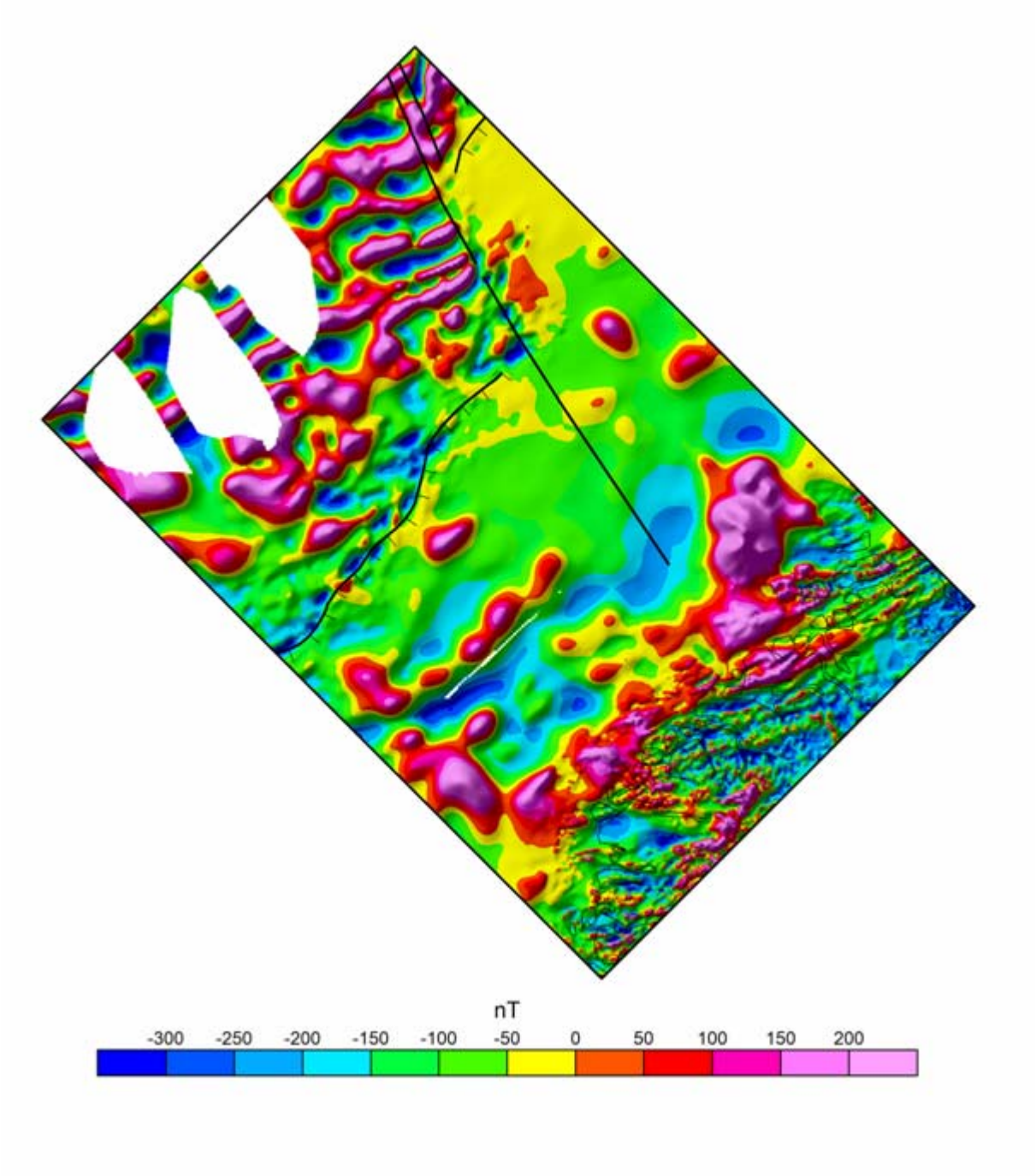

Figure 2.3 Total magnetic field map. See location of study area on Figure 2.1.

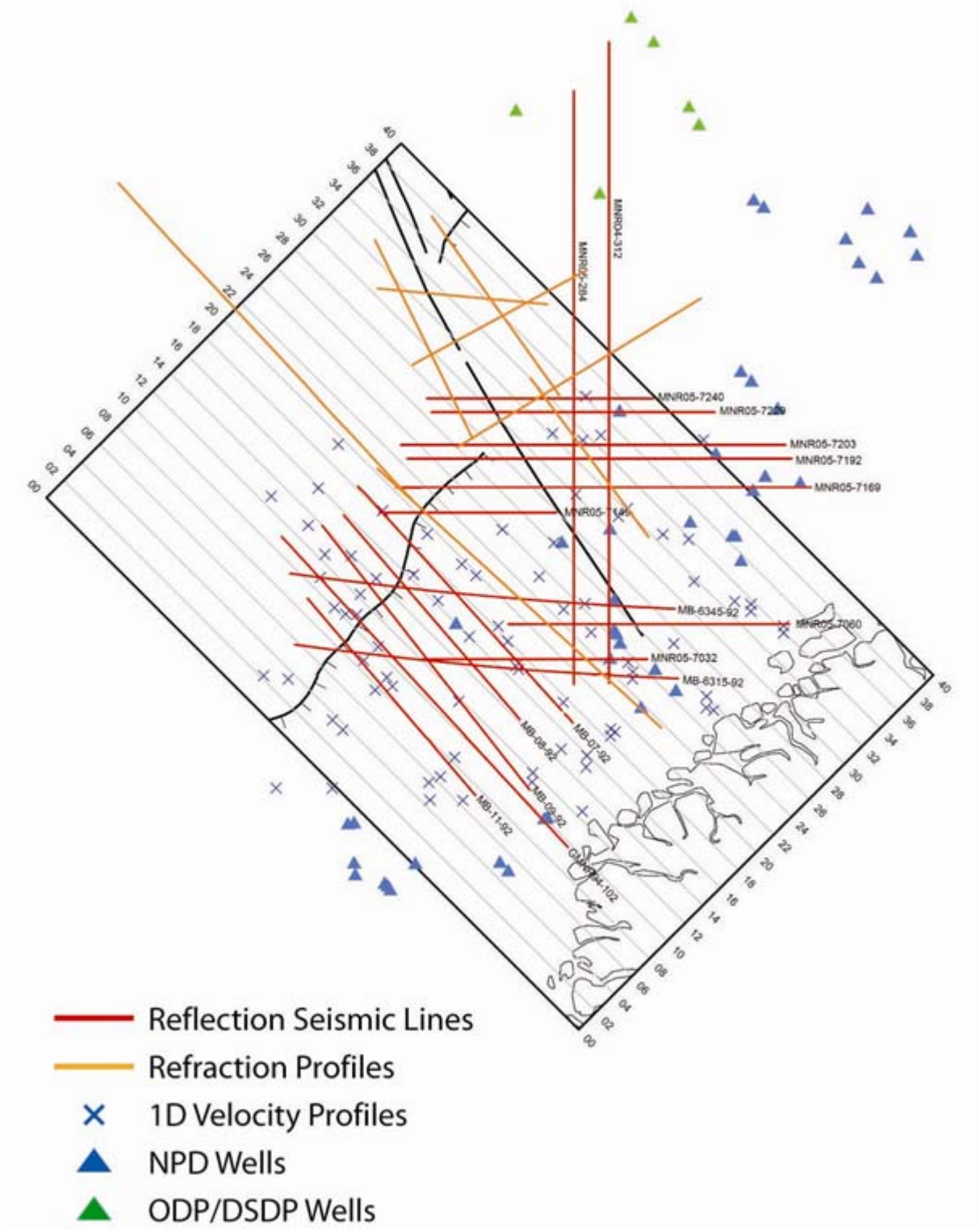

Figure 2.4 Overview of constraining data. See location of study area on Figure 2.1.

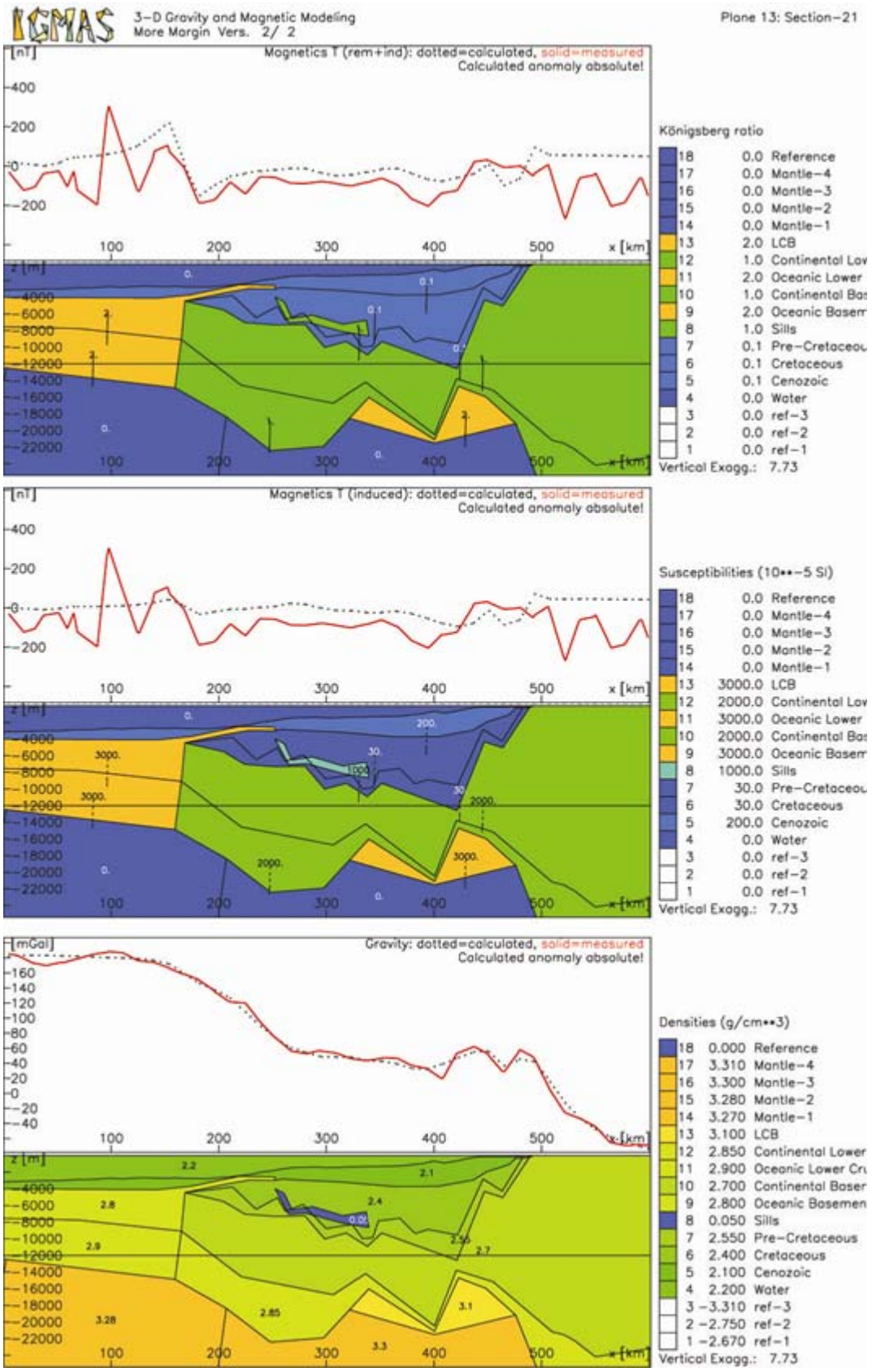

Figure 2.5 *An example of a profile in the model. This profile (section 21) is in the middle of the model (compare to Figure 2.4). a) is the remnant magnetization, b) the induced magnetization and c) is the gravity response of the density structure.*

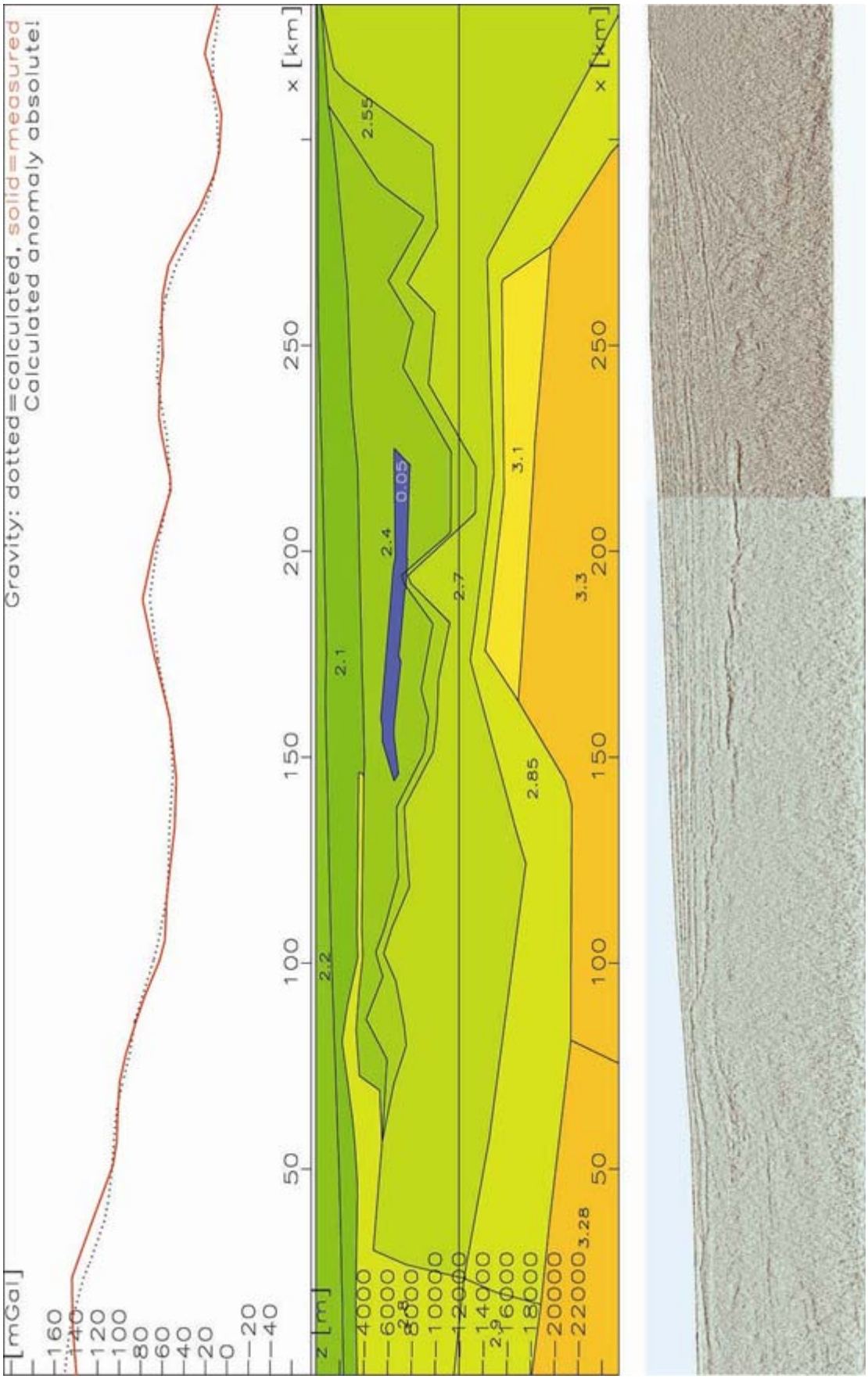

Figure 2.6 Model compared to GMNR94-102 line. The depth of the seismic line is 14 s in TWT.

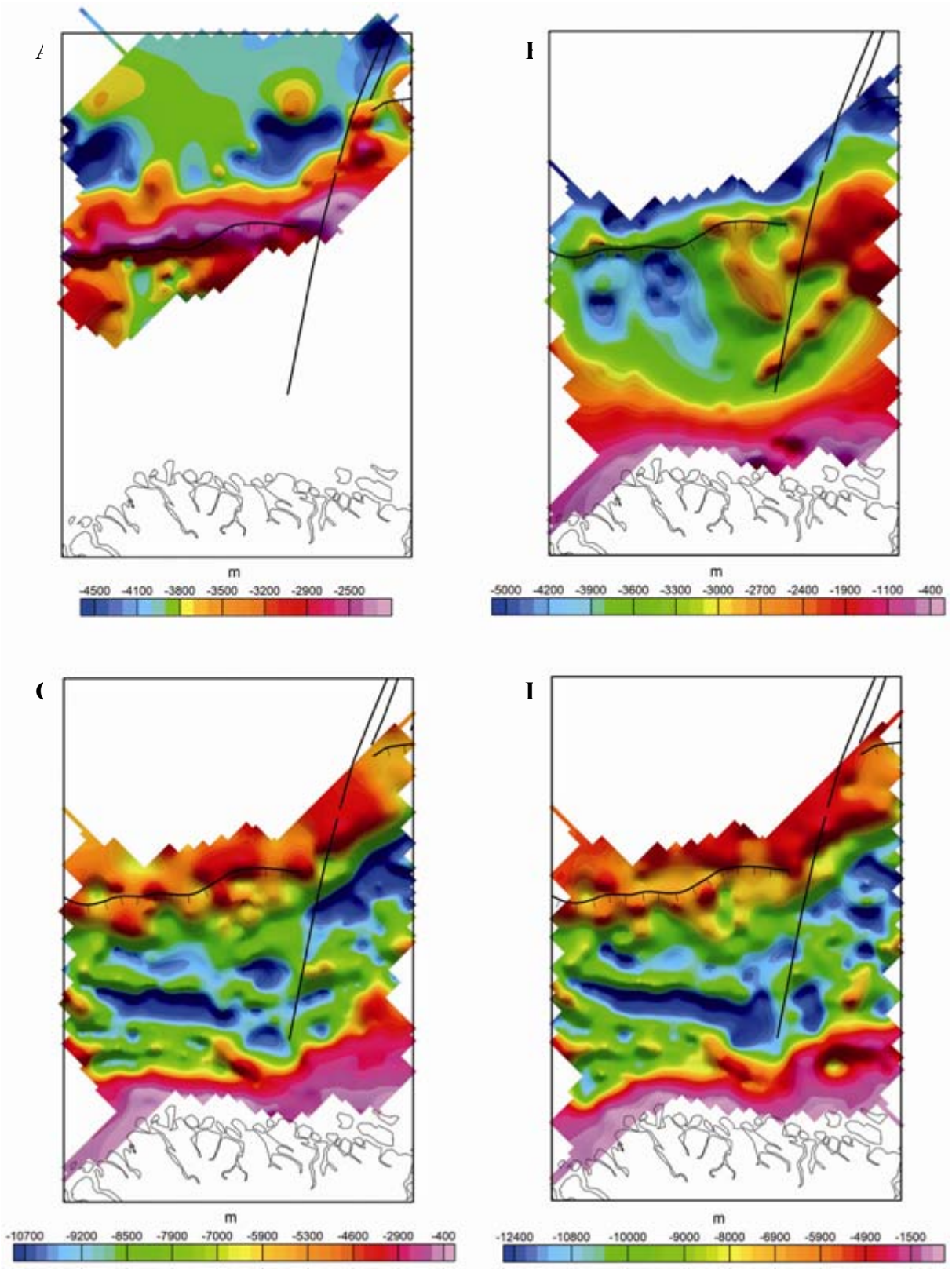

Figure 2.7 *Horizons from the model. a) Depth to top of the basalts. b) A combined map of the base of the basalts and base Tertiary. c) Depth to base Cretaceous. d) Depth to top crystalline basement. See location of study area on Figure 2.1.*

3. 3D SBL MODELLING

Stein Fanavoll, EMGS Trondheim

3.1 3D Modelling Software

For model building, Roxar's software RMS is used. This is a powerful tool, and enables creation of representative 3D models based on input from seismic interpretation.

3D modelling is carried out by use of in-house developed software. The 3D modelling program is a finite difference, time domain program, calculating the Maxwell's Equations in 3 dimensions. The program also supports anisotropy (TVI, 'TransVerse Isotropic'). However, anisotropy has not been an issue in this project.

3.2 Model Building

Based on the input from grav/mag modelling and seismic interpretation (Chapter 2), point data for each interpreted horizon was loaded into an RMS project (Figure 3.1). Some horizons consist of rather scattered data points, but to build a representative model, this was regarded as sufficient data coverage. In order to build a complete simulation grid for the 3D modelling, additional horizons had to be created. A list of all imported and created horizons is given in Table 3.1. Further, polygons are drawn to restrict the extent of layers defined only in parts of the area. These are later used when modifying the layer model after gridding. In Figure 3.1, the polygons for the basalts and the upper sill layer are shown. An overview of all polygons is given on Figure 3.2.

The imported data were gridded within a rectangle which covers the coordinates of a subsequent SBL line. RMS requires that all horizons are continuous throughout the project area; therefore all horizons were gridded inside the project rectangle, even those which were defined in a restricted area only. These horizons were later modified as described below.

After gridding, the horizons must be modified in order to avoid peculiarities and artefacts caused by extrapolation of the surfaces. The following rules have been applied in the modification:

- No horizons are allowed to cross each other. As a result of this, there is a 'hole' in the sill horizon where it was interpreted to be higher than the Base Tertiary horizon. This hole will show on the response.
- Layers which are restricted by polygons are defined only inside the polygon. Outside the polygon, the layer thickness is set to zero, and the horizons are made equal to a horizon above (reservoirs are made equal to Base Basalt and Base Sill, respectively) or below (Sills and Complexes are set equal to BCU, see example in Figure 3.3)
- Base Tertiary and the Basalt horizons are combined in a way that inside the Basalt polygon, the Base Tertiary horizon is set equal to base Basalt, outside the polygon, the

Basalt horizons are set equal to Base Tertiary. After these operations, Base Tertiary and Base Basalt were identical.

Figure 3.4 shows the resulting profile along the seismic line GMNR-94-102.

Table 3.1 Overview of imported and created horizons for the Møre Margin Modelling Study. Descriptions of how they are restricted and/or created are given in the table.

Imported horizons	**Created horizons**	**Description of modification**
	Top Model	Zero Level
Seabed		
Top Basalt		Merged with Base Tertiary outside Basalt Polygon
Base Basalt		Merged with Base Tertiary outside Basalt Polygon
Base Tertiary		Merged with Base Basalt inside Basalt Polygon
	Reservoir Level 1 (Base Basalt + 200 m)	Restricted to Reservoir 1 Polygon
Upper Sills		Restricted to Sill Polygon
	Base Sill (Upper Sill + 100 m)	Restricted to Sill Polygon
	Reservoir Level 2 (Base Sill + 200 m)	Restricted to Reservoir 2 Polygon
Lower Sill Complexes		Restricted to Complex Polygon
	Base Complexes (Top Complexes + 100 m)	Restricted to Complex Polygon
Base Cretaceous		
Basement		
	Base Model	Deepest point of model

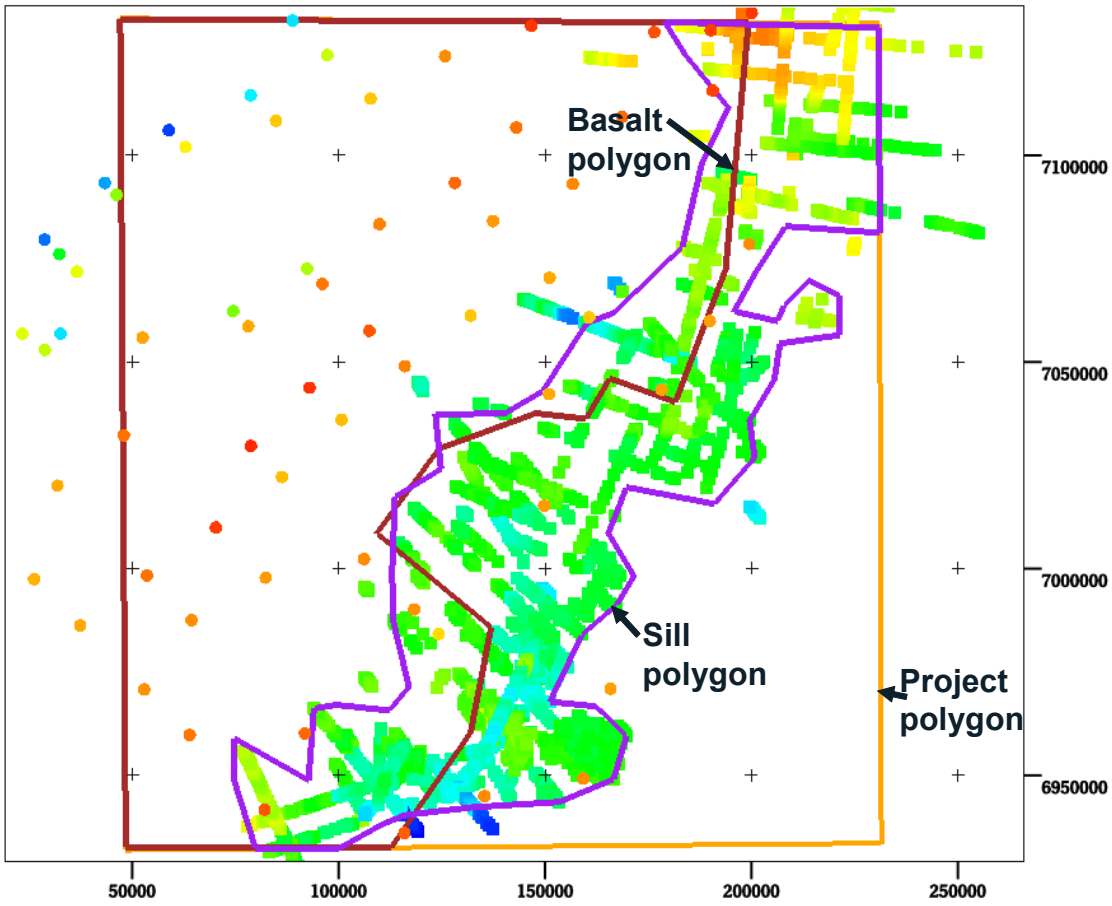

Figure 3.1 *Imported point data from seismic interpretation (see previous chapter). Examples on this figure are Base Basalt (scattered points) and Upper Sill (dense points). Based on the distribution of the input points, polygons are drawn to restrict the extent of the different layers.*

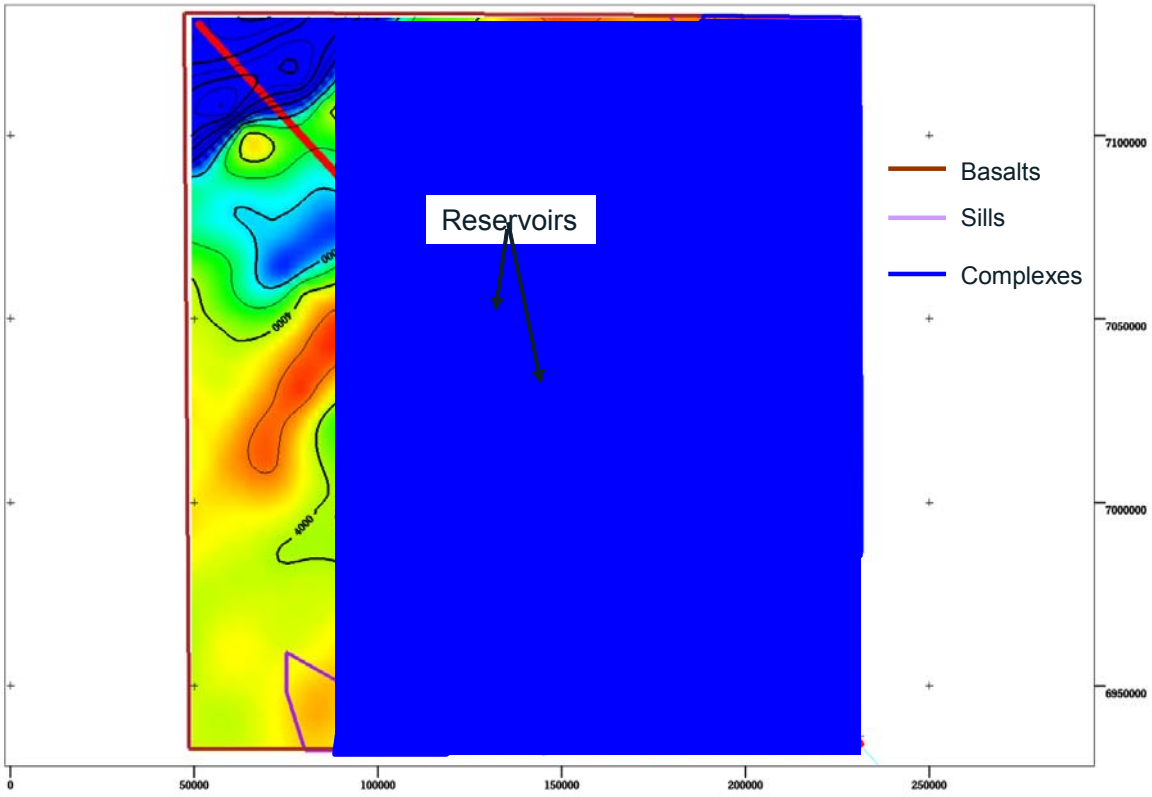

Figure 3.2 *Overview of all polygons used for the model building in the project. In addition to the polygons of the basalts, sills and complexes, two hypothetic reservoirs are added, in order to check the sensitivity in the model to such volumes.*

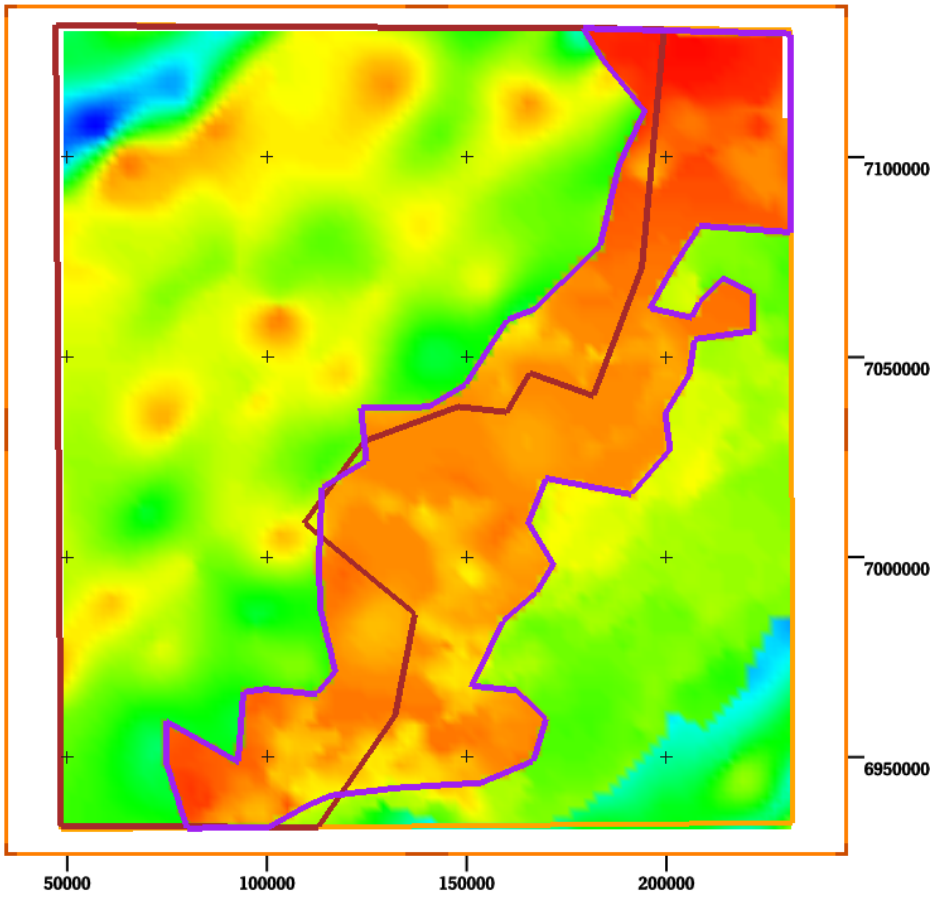

Figure 3.3 *Gridding of the Upper Sill horizon. Outside the defined Sill polygon, the horizon is set equal to the deeper BCU horizon.*

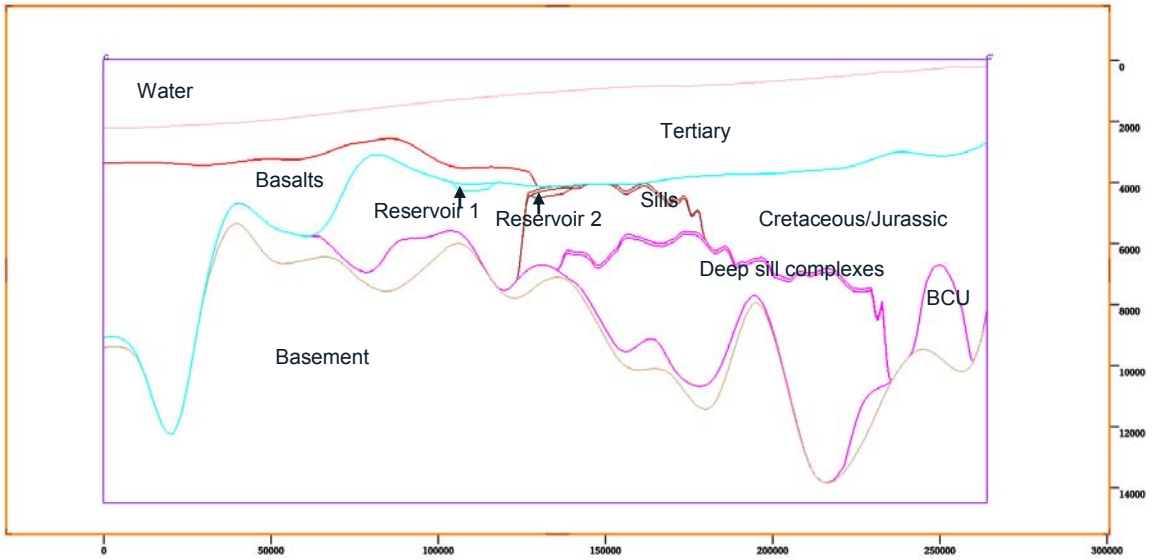

Figure 3.4 *Resulting profile along the seismic line GMNR-94-102.*

3.3 Output resistivity grids

After construction of the layer model, the next step is to assign resistivity properties to each layer. Having very little information of the resistivities in the area, this parameter is the most uncertain.

In the study area, three main high resistive rock types are present: sill intrusions, flow basalts and basement. The resistivity of sills are known to be very high (ref. well 6607/5-1 (Utgard High) encountering a 90 m dolerite of 1400 Ωm from log values (NPD fact pages)). The model is using 500 Ωm for the sills. Flow basalts have been expected to have lower average resistivity due to the fact that it has been exposed, which makes it subject to weathering and sedimentation of e.g. ashes and clastics, making the average resistivity lower. In the initial model, 100 Ωm has been used for the basalts. Basement has normally high resistivity, ranging from some tens in the upper, weathered part, to thousands further down. However, Basement is the lowest layer in the model, thus acting as an infinite halfspace downwards. Experience from earlier modelling studies indicates that the modelling results are not very sensitive to halfspace resistivity, as long as it is considerably higher than the overburden. In the model, 50 Ωm is used.

In addition to these layers, a reservoir resistivity of 60 Ωm is used when modelling hydrocarbon reservoirs. Background resistivities are typically between 1 and 3 Ωm. We have used 1.5 Ωm for the Tertiary section, and 2 Ωm for the Cretaceous/Jurassic section.
An example of a resistivity profile is shown in Figure 3.5.

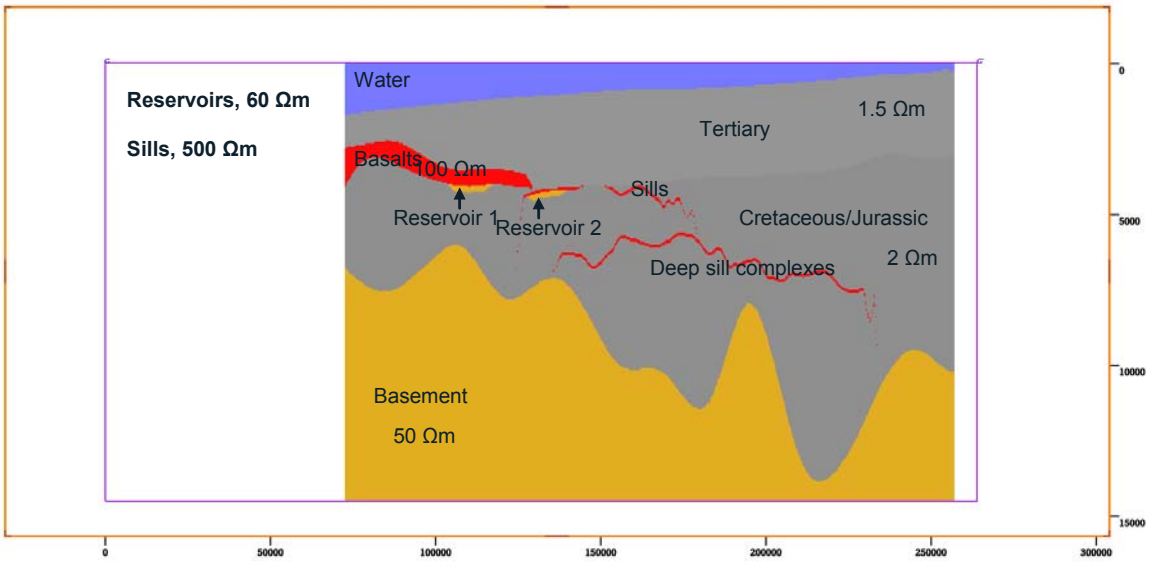

Figure 3.5 Initial model used in the 3D modelling.

3.4 3D Modelling and processing

Three different scenarios were run in the 3D modelling process:

1. Base model, as shown in Figure 3.5. This model is run also with hydrocarbon reservoir,
2. New model with reduced resistivity in Basalt, Upper Sill and Basement
3. Model with added thickness in Basalt

Modelling was run with three frequencies, 0.1 Hz, 0.25 Hz and 0.75 Hz.
The three models are described in Figure 3.6.

Figure 3.6 *The three models used in the study, left: initial model, middle: new model with reduced resistivity in basalts, sills and basement, right: model with increased thickness of basalts. The two first models were run both with and without hydrocarbon reservoirs.*

3.4.1 Up-Down separation

As seen on Figure 3.6, the water depth varies considerably along the line. In the western end, the water depth is more than 1500 m, while in the eastern end it is 200 m. Such water depth variations will inevitably result in an SBL response in itself (commonly denoted as the 'air wave'), which may mask responses from subsurface resistivity variations. The influence of the air wave can be observed on single receivers. On Figure 3.7, two receivers from each end

of the survey line (Receivers 54 and -10) are shown. At increasing offsets with increasing frequencies, a bend is observed on Receiver 54. This is due to the air wave.

One way of reducing such a problem, is through processing to reduce the effect of the air-wave, which is the wave field caused by the air water interface. This process, called Up-Down separation, ideally removes the down going wave field and leave us with the field generated in the subsurface. This process has some limitations, assuming a plane layer earth, and that the resistivity of the upper layer is known. These assumptions are of course better fulfilled in a modelling scenario. Up-Down separation was applied to the data for all scenarios in order to show response variations along the line not affected by bathymetry. In Figure 3.8, the result of Up-Down separation is shown for Receiver 54 and Receiver 12. The phase curves for Rx54 are now straightened out, while only minor changes can be seen on Rx12.

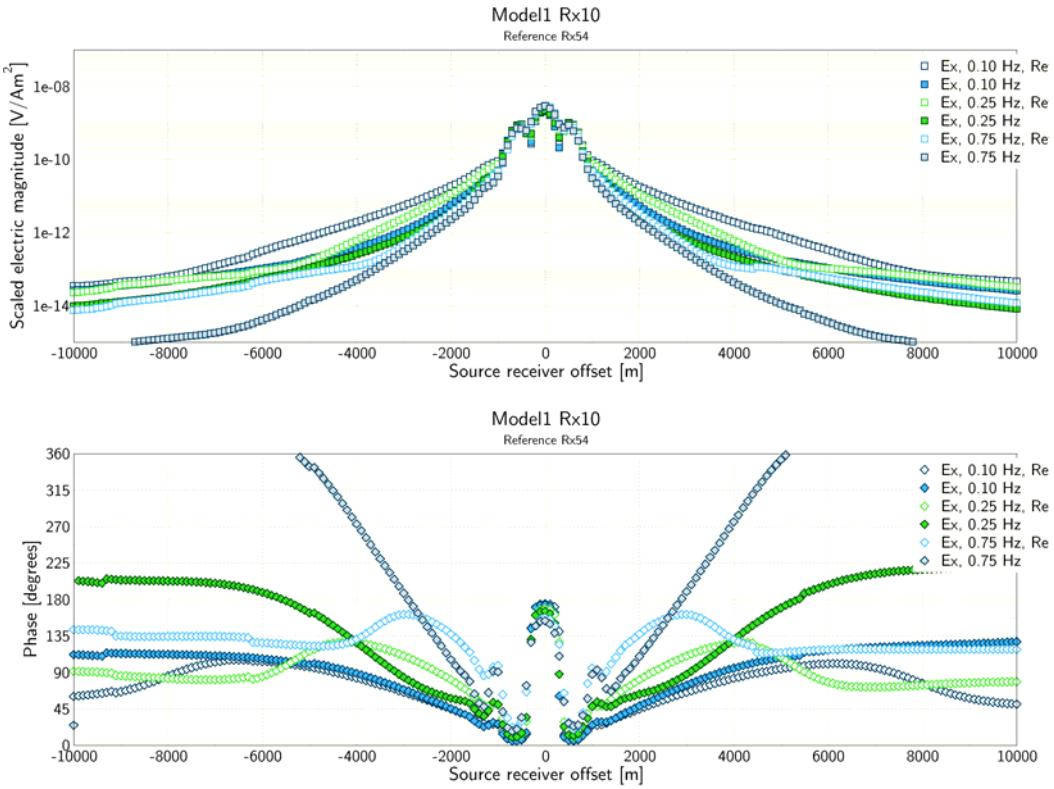

Figure 3.7 *Comparison of Receivers 54 (open symbols + Re) and – 10 (closed symbols). The bend seen on Rx54 is due to the air wave.*

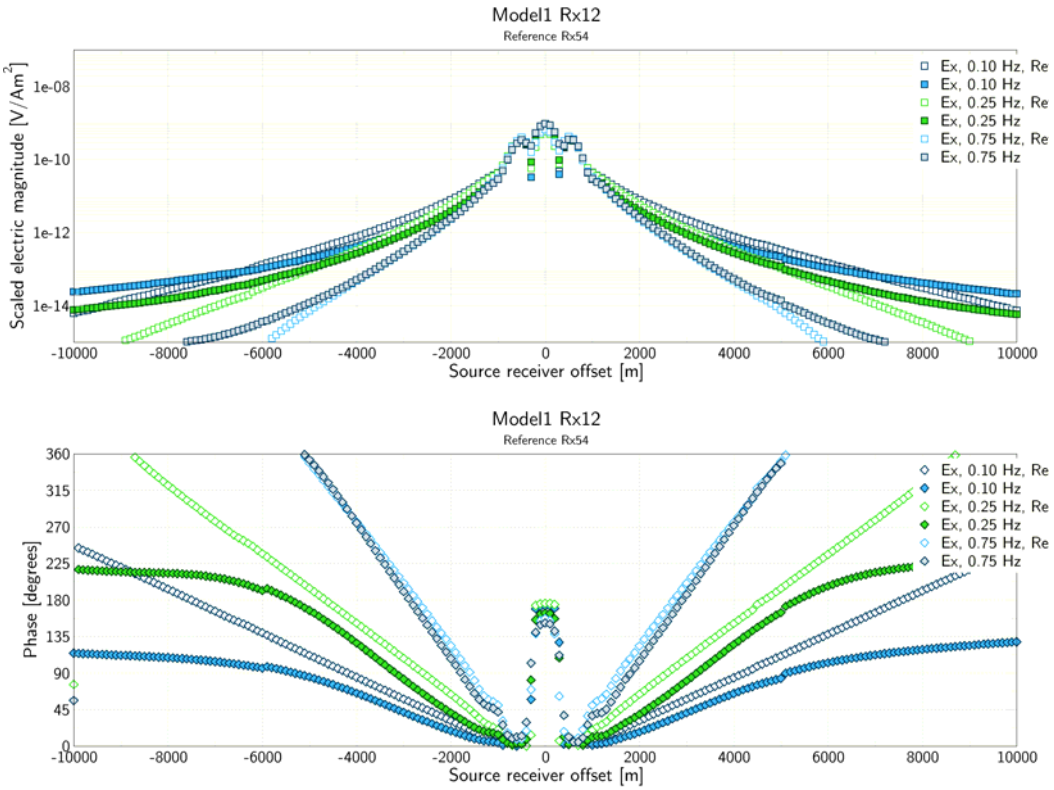

Figure 3.8 *Comparison of Receivers 54 (open symbols) and – 12 (closed symbols), after Up-Down separation. The bend seen on Rx12 is now due to subsurface resistivities.*

3.4.2 Reference receiver

SBL measurements are designed in order to record variations in the measured electromagnetic field along a transect, or within a specific area. The reference for these variations is a (synthetic or real) receiver in an area where the influence from high resistive layers is as little as possible. The selected reference in this study is Receiver 54, on the south-eastern (out-tow) side. This is an area outside the intrusions (see Figure 3.9), and the Basement is also deep in the area. The reference receiver is shown in Figure 3.10, before as well as after Up-Down separation.

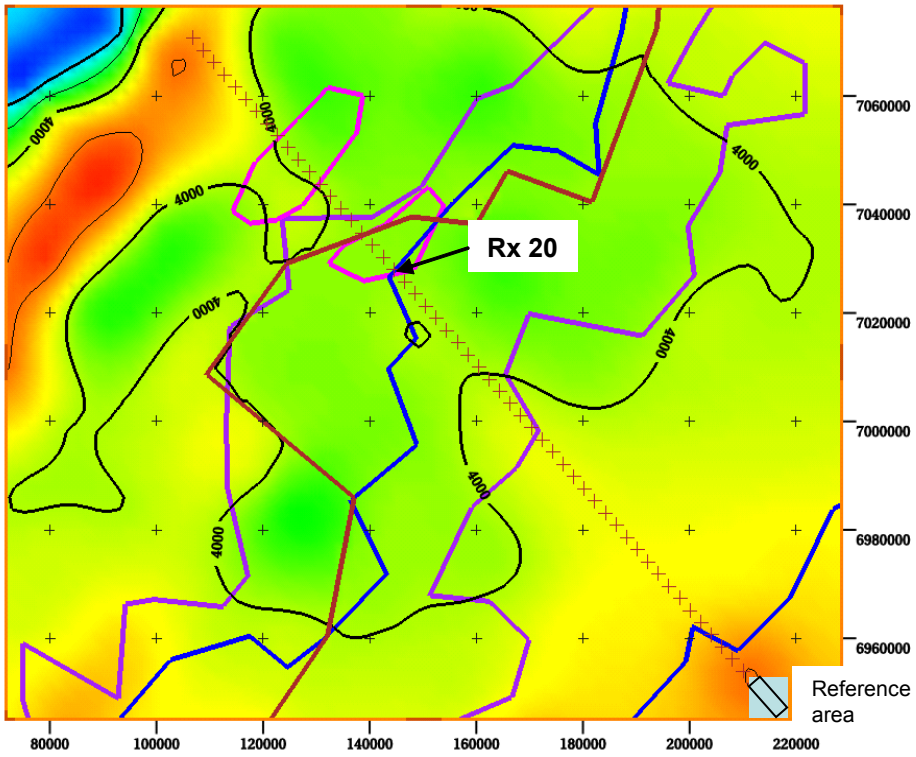

Figure 3.9 *Layout of the 54 receivers. Receiver 1 is to the north-west. Location of the reference area in the south-east (Rx53, out-tow) and the example receiver in Figure 3.11 (Rx20) is also shown.*

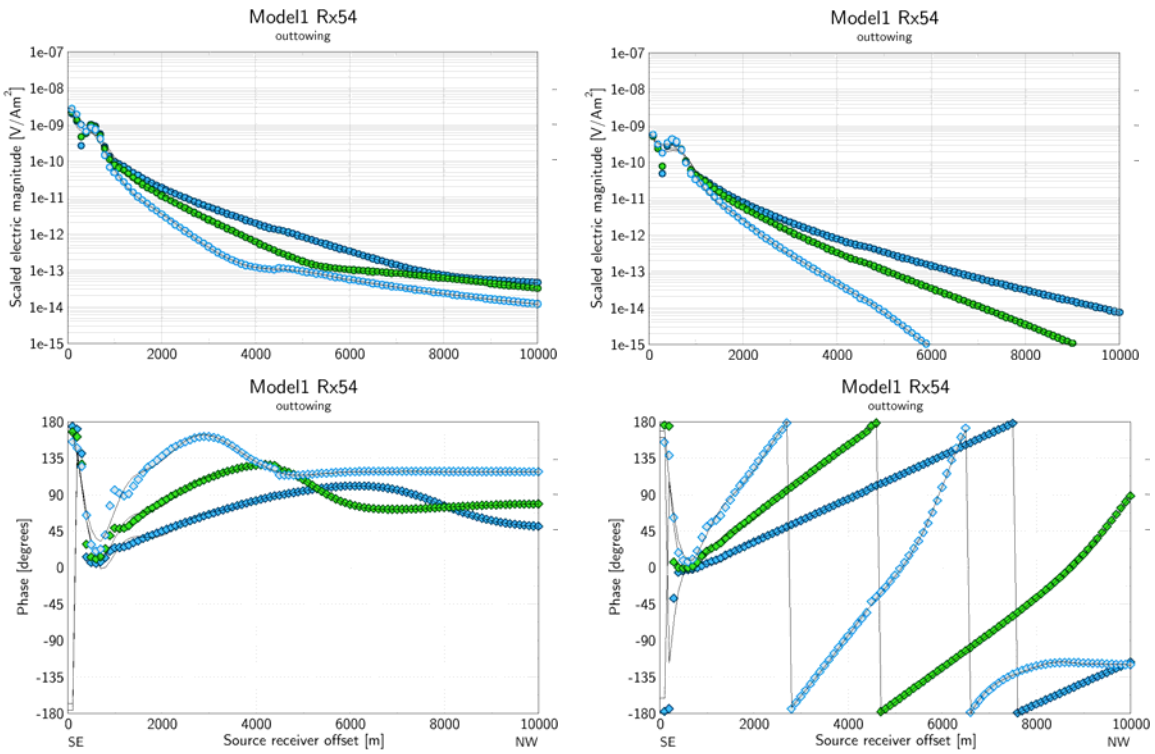

Figure 3.10 Reference receiver (Rx54) before (left) and after (right) Up-Down separation. The reference is represented by a 'best fit' curve for normalisation.

3.4.3 Normalisation

In order to better visualise the lateral variations, all receivers are normalised with respect to the reference receiver. This is carried out by dividing the magnitudes and taking the difference between the phase curves. This results in normalised plots for each receiver, as seen in Figure 3.11 for Receiver 20.

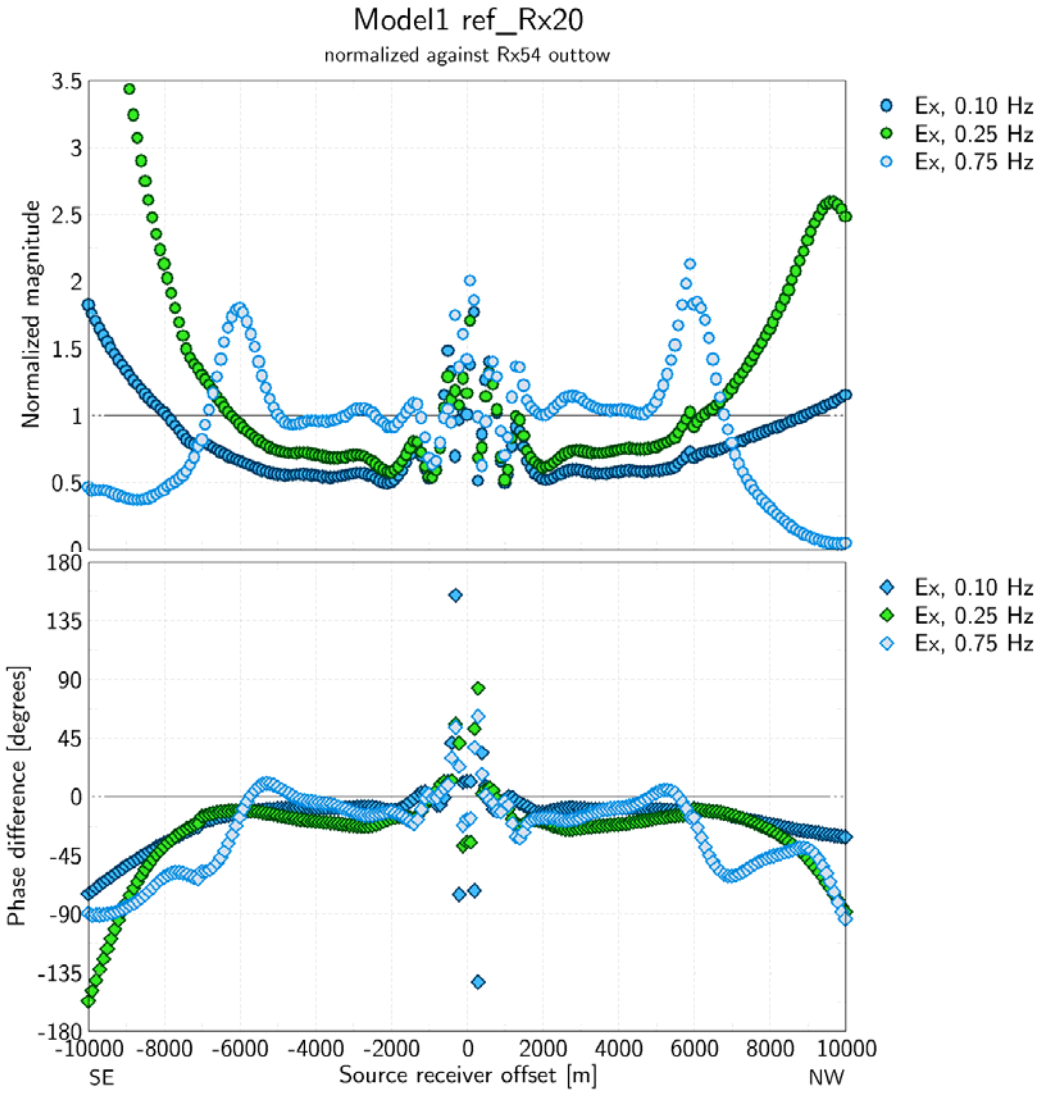

Figure 3.11 Normalised magnitude (upper) and phase difference (lower) for Receiver 20.

3.5 Results

3.5.1 Summary plots

In order to present the results for the whole line, summary plots are generated for a number of offsets. For a specific offset, the median normalised value in a range around the offset is posted at half the offset position relative to the receiver. This is done for all receivers in an SBL line. The resulting plots then show the variations in the response along the line. In

Figure 3.12, summary plots for short offsets (2000 m and 4000 m) are shown before and after Up-Down separation. On these plots, the bathymetry effect is the most prominent, although a response from the shallowest part of the Basalt is seen in the western end of the line. This response is mode pronounced for the phase than for the magnitude. We see that the Up-Down separation reduces the air wave effect but not completely. This may be due to the fact that some energy connected to the water layer is not vertical (e.g. reflections) and hence is not effectively removed. The air wave effect will overprint other responses also at larger offsets. Therefore only Up-Down separated results will be shown for the remaining part of the report.

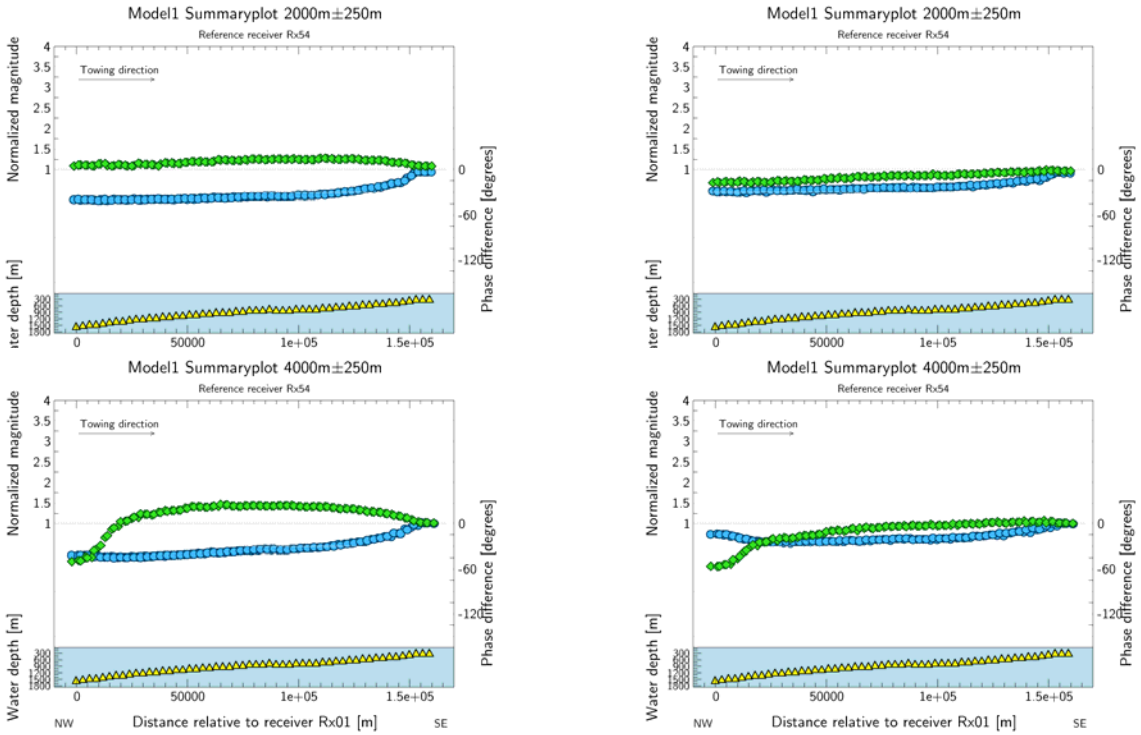

Figure 3.12 Line summary plots before (left) and after (right) Up-Down separation for 2000 m (upper) and 4000 m (lower) offsets. The bathymetry effect is clearly reduced after Up-Down separation. In the western part of the line, response from the Basalt is seen.

On larger offsets, a response from the upper sill and the basalt is clearly seen (Figure 3.13). Also, the 'hole' in the sill layer is seen as a notch in the plot. The start of the basalts is easily seen on the plots. However, the point where they get considerably shallower in the western part (Figure 3.14) gives the largest response. Due to the exponential attenuation of the signal, the response from a layer at 1100 m depth will be considerably larger than from a layer at 2250 m depth. The shallowing of the basalts is also the reason why they give a response at 4000 m offset (Figure 3.12). The responses are increasing with increasing frequency and offset.

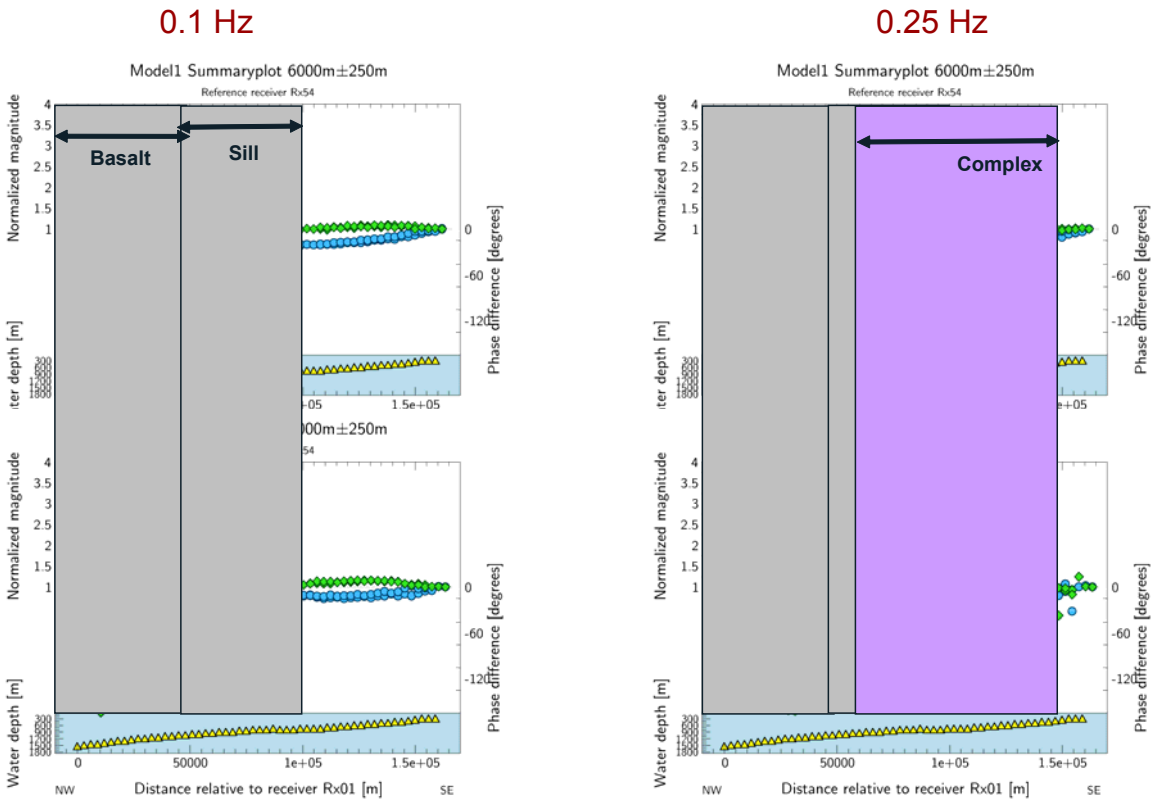

Figure 3.13 *Line summary plots for 0.1 Hz (left) and 0.25 Hz (right) for 6000 m (upper) and 9000 m (lower) offsets.*

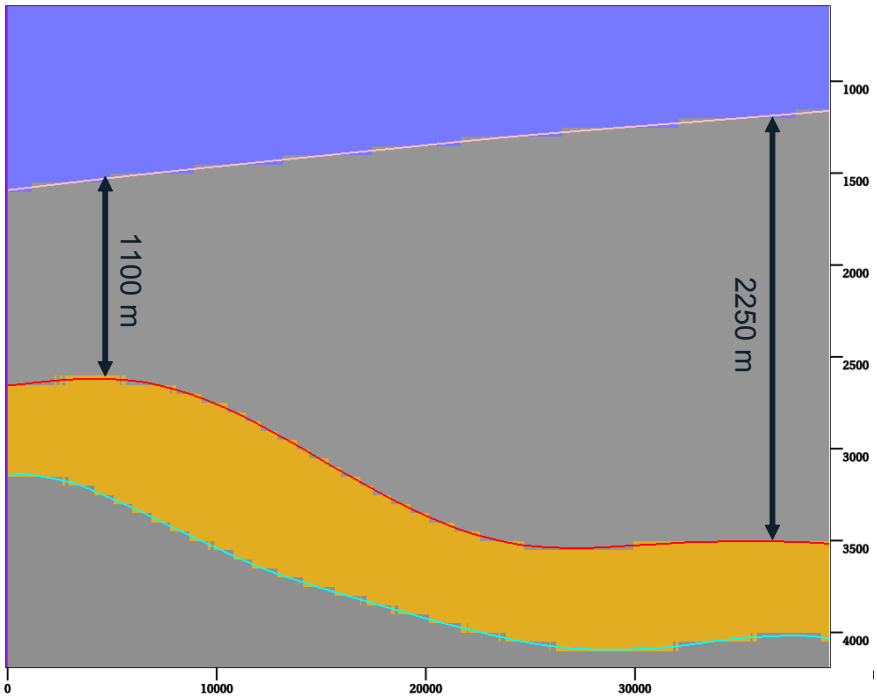

Figure 3.14 *Shallowing of basalts in the western part of the line.*

3.5.2 Revised model (Model 2)

In order to test the sensitivity to variable properties in the subsurface, an alternative model was created. In this model, the resistivity in the basalts was set to 50 Ωm (from 100), the upper sill layer to 200 Ωm (from 500) and the Basement to 20 Ωm (from 50). The change in response is visible as seen on Figure 3.15, but not to a linear scale with respect to the change in resistivity.

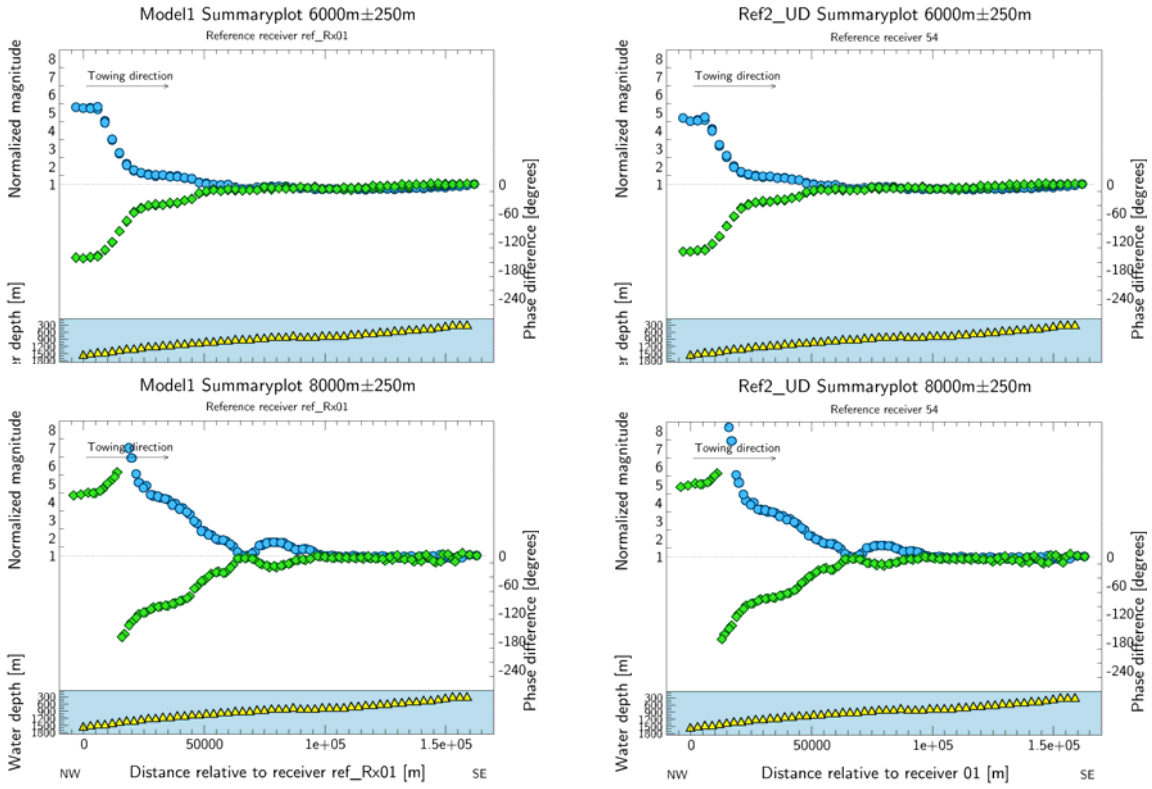

Figure 3.15 Comparison of summary plots for Model 1 (left) and Model 2 (right), for 6000 m (upper and 8000 m (lower) offsets.

In order to visualise the changes inferred by the revised model, we can make a new summary plot by normalising each receiver from the new model by the respective receiver from the first model. This process will show only the response caused by the differences in the two models, and will also eliminate the bathymetry issue. This process is denoted "Receiver by Receiver Normalisation" (Rx/Rx Normalisation). The result of this normalisation is shown in Figure 3.16, for two offsets and two frequencies (0.1 Hz and 0.25 Hz).

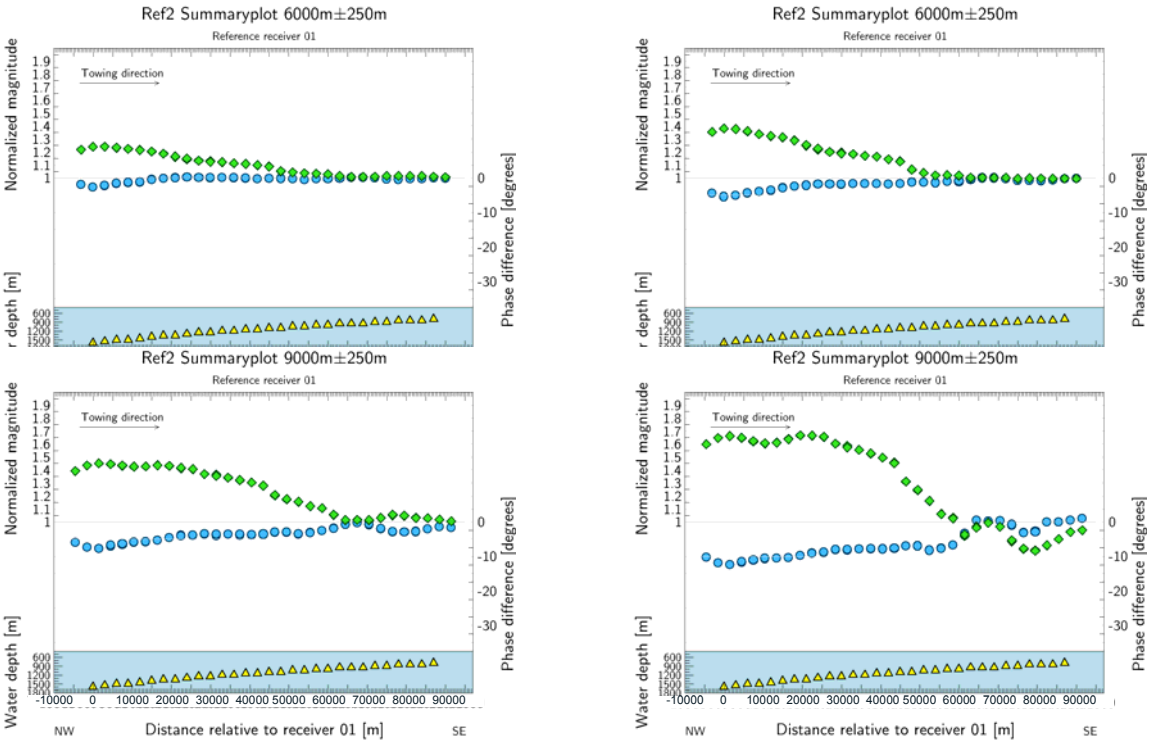

Figure 3.16 Rx/Rx normalisation for the revised model with lower resistivities in the basalts, sills and basement. The difference increases with increasing frequency and offset. The frequencies are 0.1 Hz (left) and 0.25 Hz (right). Note the scale.

3.5.3 New model with increased thickness of basalts (Model 3)

In order to further evaluate the sensitivity of the modelling to the properties in the basalt layer, a third model was constructed, with increased thickness of the basalt with 500 m. this implies a thickness approximately twice as large as the initial model (Figure 3.17). Resistivities were kept as in the original model. The results are shown in Figure 3.18 and Figure 3.19. Comparison of line summary plots from this model with the initial model shows hardly any differences. However, Rx/Rx normalisation shows minor differences, but partly as negative differences, which is opposite to what one should expect from the models. Obviously, results are not sensitive to increased thickness in a high resistive basaltic layer of considerable thickness. The reason for this may be that having already a large 'resistive volume' in Model 1, increasing the thickness may cause the guiding of the energy in the resistive layer to be less efficient. Hence, the modelling results may be somewhat unpredictable.

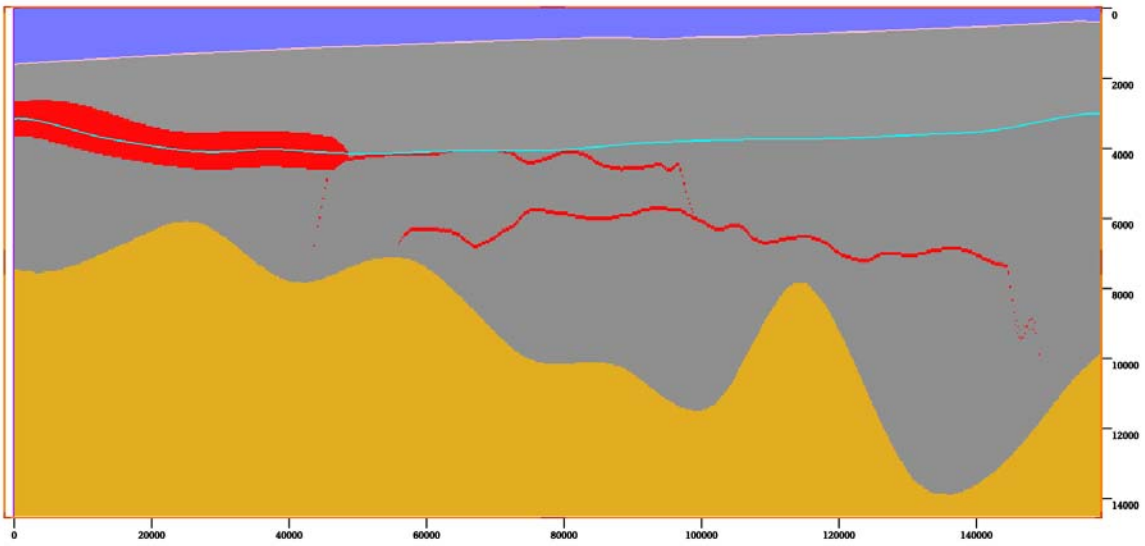

Figure 3.17 Model 3 with increased (500 m) thickness of the basalt layer. The Base Basalt horizon is shown in blue to illustrate the initial thickness.

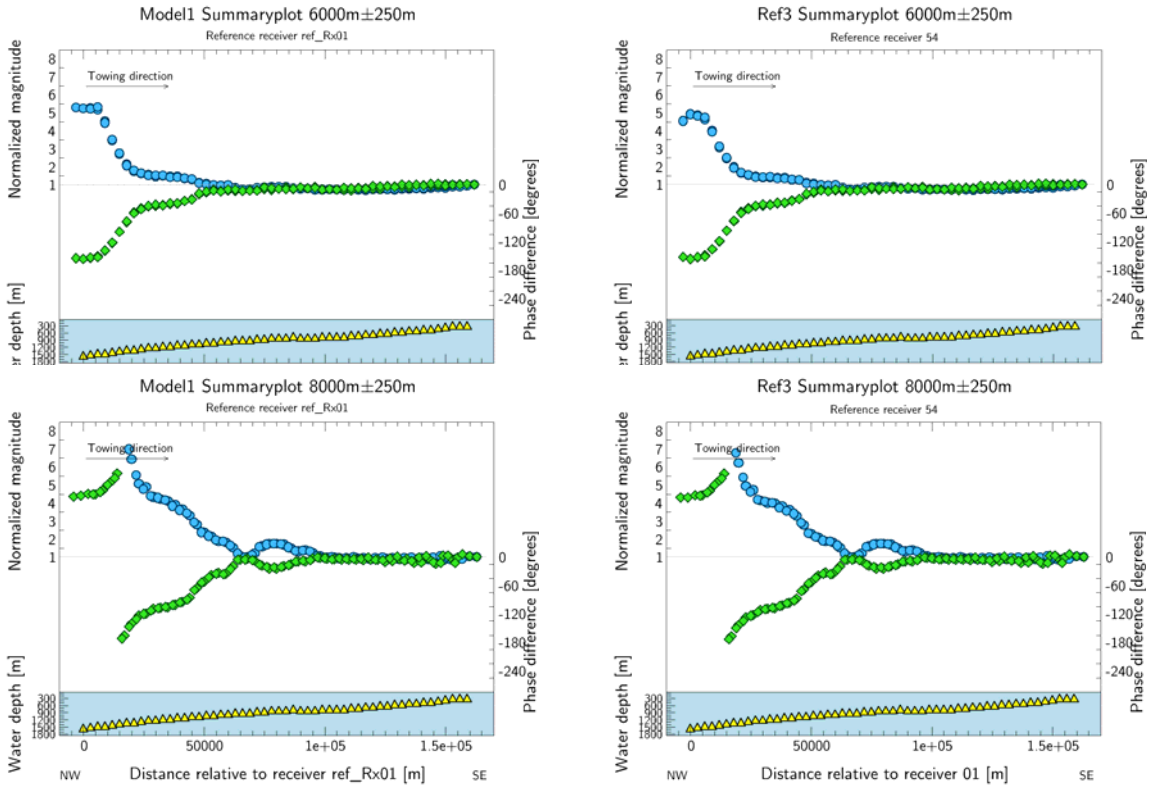

Figure 3.18 Comparison of summary plots for Model 1 (left) and Model 3 (right), for 6000 m (upper and 8000 m (lower) offsets.

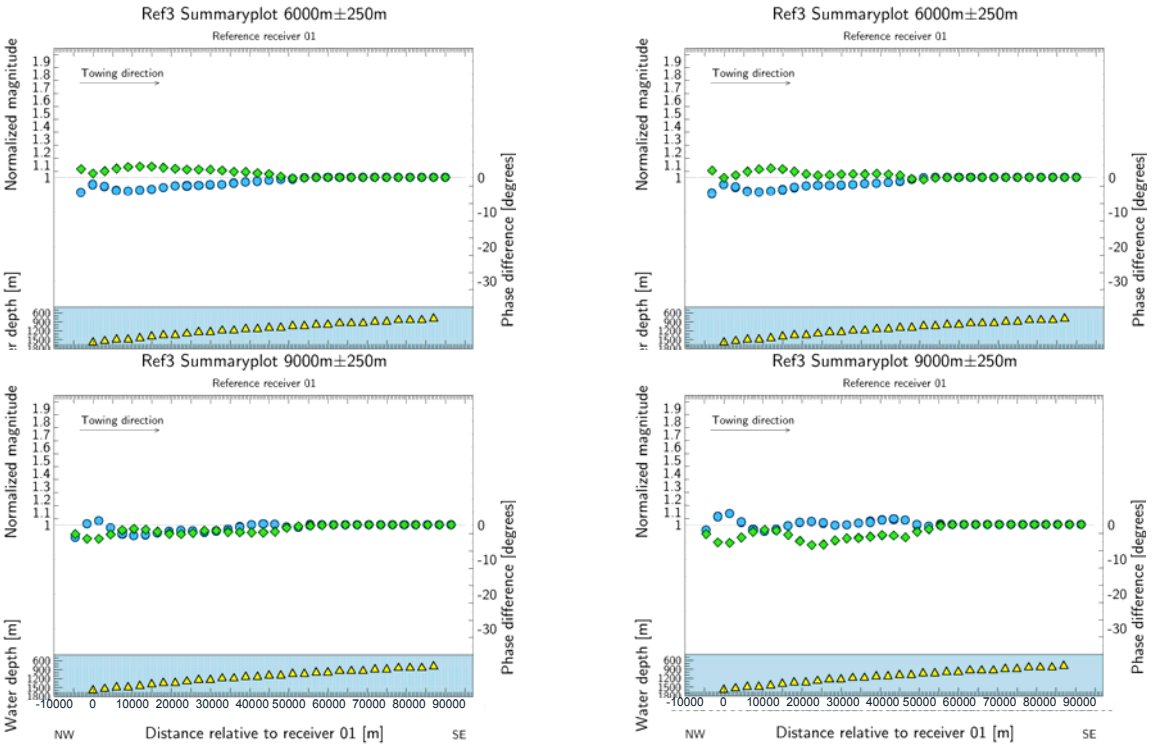

Figure 3.19 Rx/Rx normalisation for the revised model with lower resistivities in the basalts, sills and basement. The difference increases with increasing frequency and offset. The frequencies are 0.1 Hz (left) and 0.25 Hz (right). Note the scale.

3.5.4 1D Modelling of Thickness Variations in Basalts

In order to better understand the results above, 1D modelling was carried out on models with variable thickness of the basalt layer. The models are shown in Figure 3.20, and the applied frequency was 0.1 Hz.. The results (Figure 3.21 and Figure 3.22) show that for the thinner models (100, 200 and 500 m) there is an increase in response with increasing thickness (Figure 3.22) on long offsets, which is not the case for shorter offsets. For offsets up to 6000 m, there seems to be a general decrease. The thicker cases show a different behaviour, with a decrease on short offsets, and a steeper increase on longer offsets. However, neither of the thick cases (1000 m and 2000 m) gives larger responses than the 500 m case, even on long offsets up to 10 km.

The most likely explanation is that there is less guiding of the electromagnetic field when the layer gets thicker, and consequently, more energy is lost in a downward direction and less energy is sourced back to the surface. Hydrocarbon reservoirs rarely exceed 200 m in thickness, and will not behave in this way.

Figure 3.20 Simple model used for 1D modelling of variable thickness in the basalts.

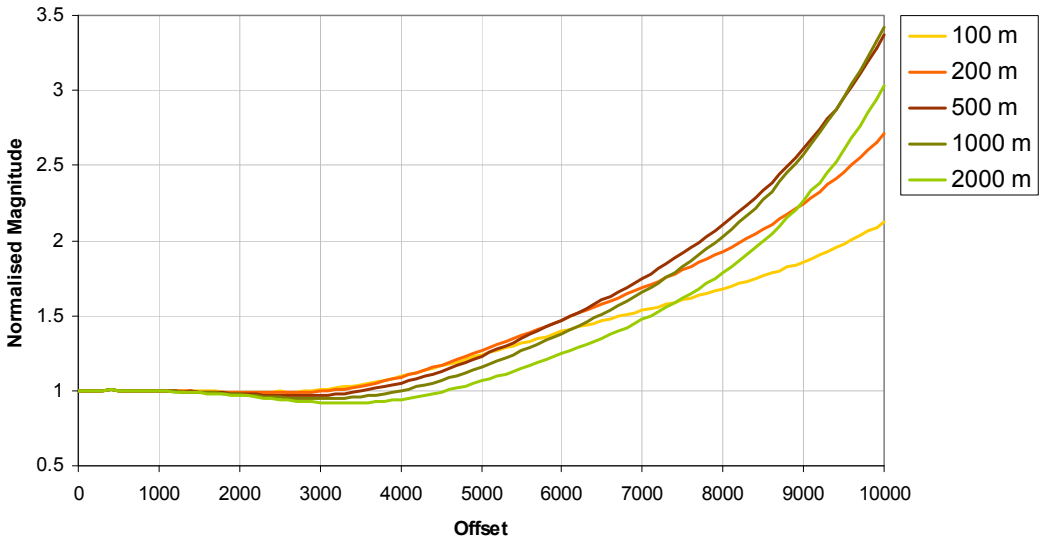

Figure 3.21 1D modelling results for 5 different thicknesses of the basaltic layer. The results show that there is an increase in response on long offsets for the thinnest models, while the two thickest have a different behaviour.

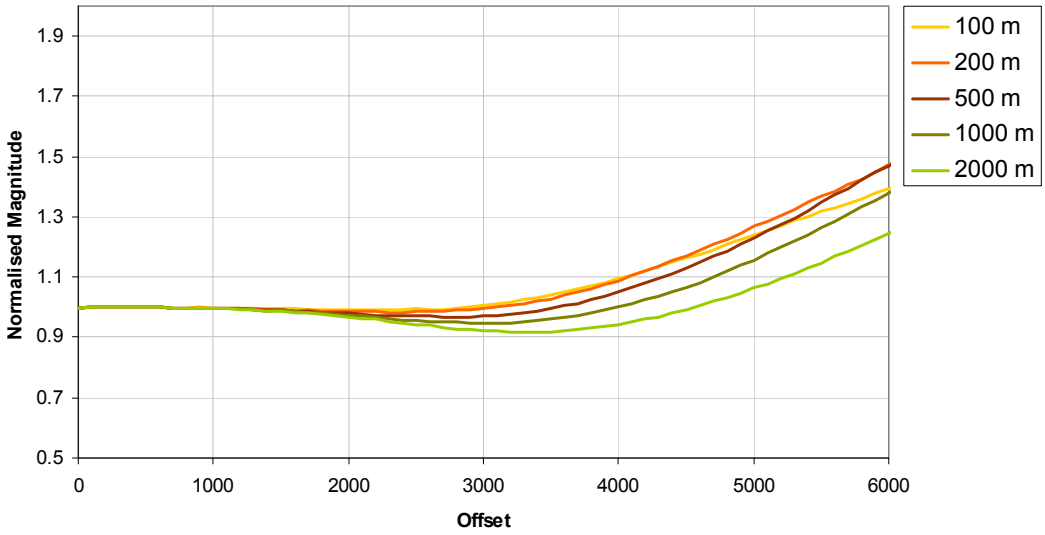

Figure 3.22 *Close-up from Figure 3.21. On shorter offsets, there is a decrease in response with increasing thickness.*

3.5.5 Detection of resistive bodies below volcanics

The presence of high resistive volumes in the subsurface, like volcanics, salt and basement, is known to reduce the relative SBL contribution from potential hydrocarbon reservoirs. The reduction is dependant on the properties (thickness and resistivity (='resistivity volume')) of the other high resistive layers.

In Model 1 and -2, hydrocarbon reservoirs were added to test this effect. One reservoir was below the basalts, while another was put below the upper sill. The reservoirs were large, approximately 10x30 km and 10x 20 km, respectively, with thickness of 200 m and resistivity of 60 Ωm.

The results are shown in Figure 3.23 – 3.25. Comparison of line summary plots (Figure 3.23) show virtually no difference between the two models. Rx/Rx normalisation of Model 1 shows small anomalies with a maximum of 1.15 at the position of the reservoirs (Figure 3.24). Rx/Rx normalisation of Model 2 (Figure 3.25) shows only a minor increase, up to 1.2. Hence, even large reservoirs can barely be detected by EM, and only when the background model is known. Normally, the magnitude of the anomaly is smaller than the uncertainty connected to the model itself.

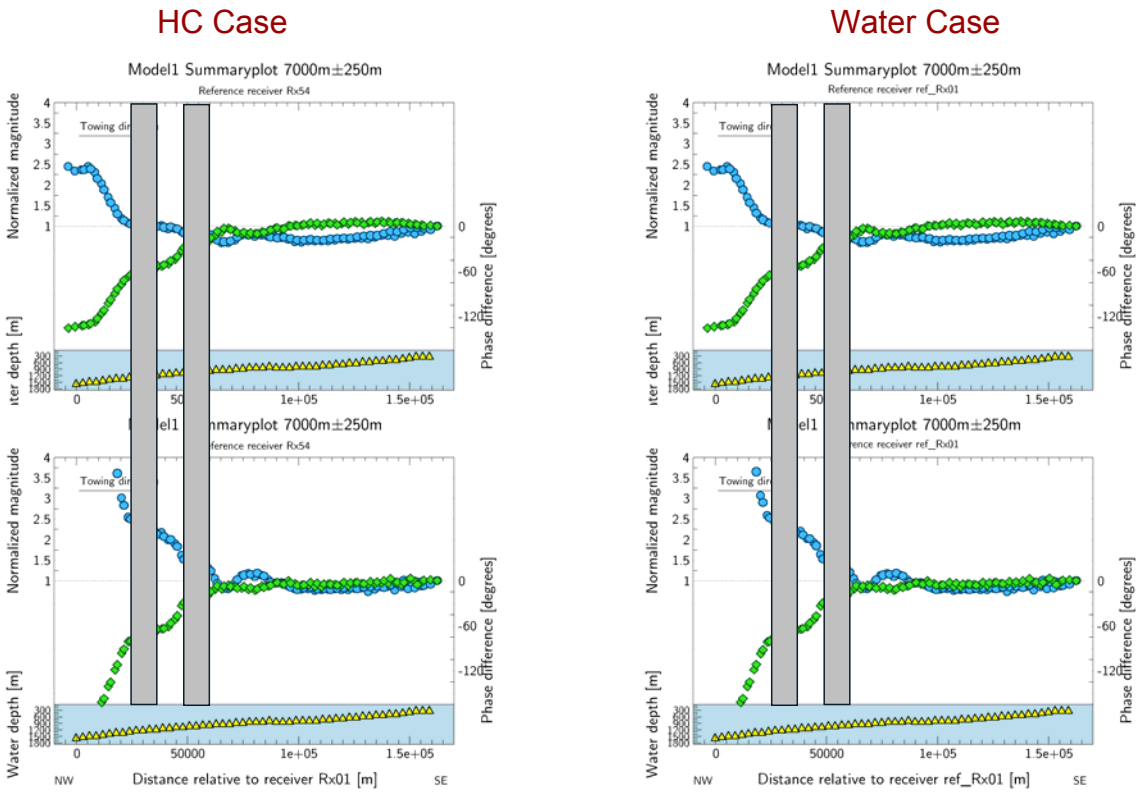

Figure 3.23 Comparison of line summary plots for a hydrocarbon case and a water case (Model 1), 0.25 Hz.

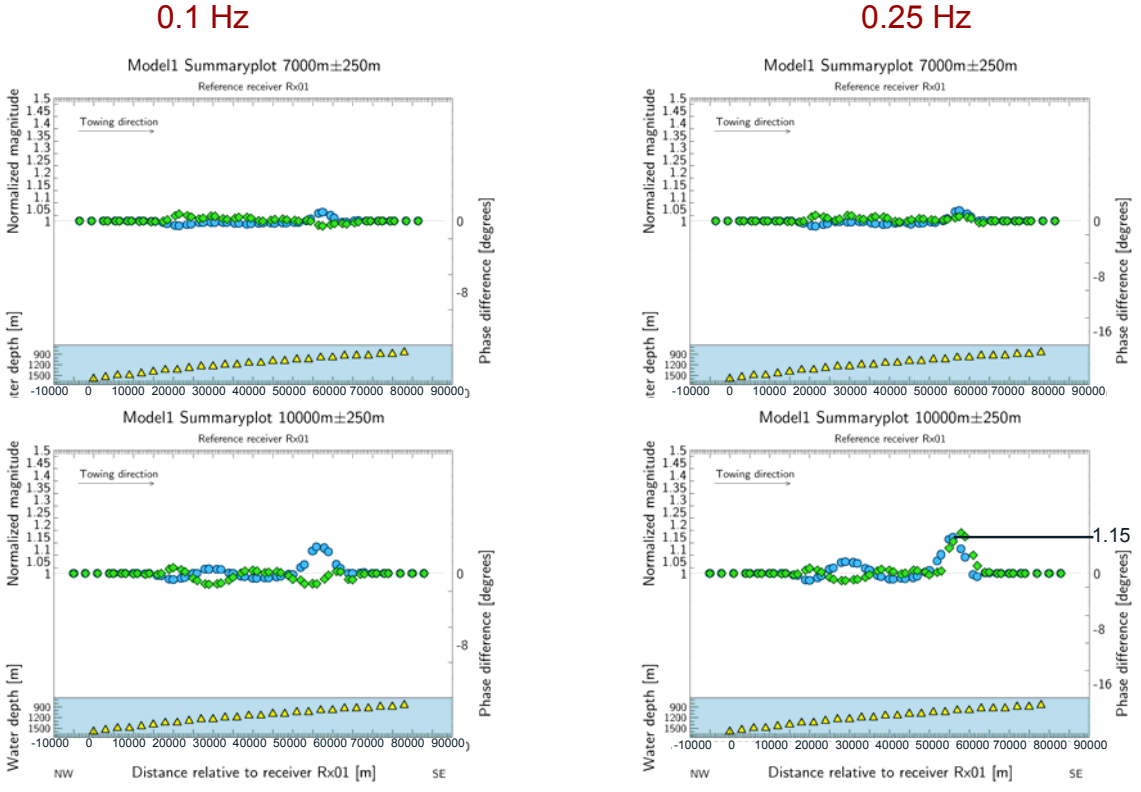

Figure 3.24 Rx/Rx normalisation of the hydrocarbon case against the water case, Model 1. The responses are very small.

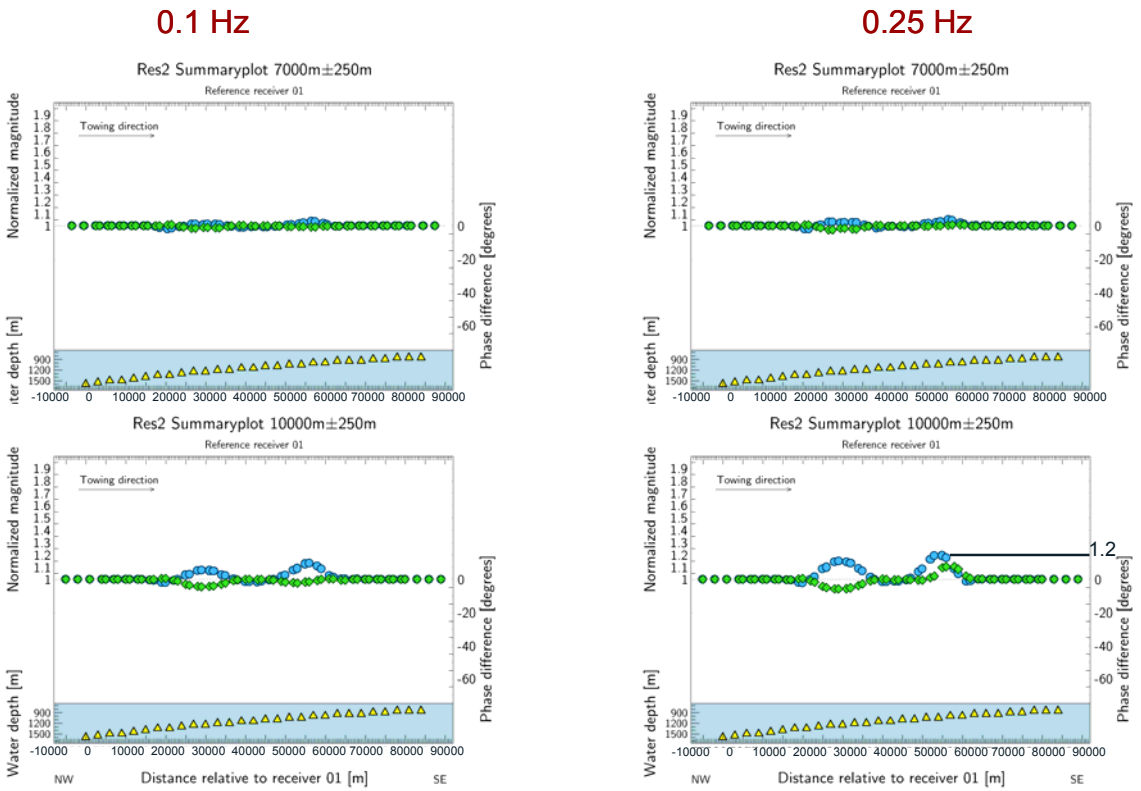

Figure 3.25 Rx/Rx normalisation of the hydrocarbon case against the water case, Model 2. The responses are slightly larger than for Model 1.

3.6 Summary and discussion of EM results

Based on gravity/magnetic modelling and seismic interpretation, a layer model has been constructed in RMS.
Three different models have been run through the emgs 3D modelling software:

- Model 1: initial model with resistivities from internal discussions
- Model 2: modified model with reduced resistivities in basalts, sills and basement
- Model 3: Model 1 with increased thickness of basalts

The main results can be summarised as follows:

- The upper sill layer and the flow basalt layer give good anomalies. However, the main response is seen where the basalts get shallow below seafloor.
- Reduction of the resistivity in the basalts and sills give a lower response, but the reduction in the response is not proportional to the reduction in resistivity.
- Increase of the basalt thickness gave little influence on the response. This may be due to less efficient guiding of the electromagnetic field in the resistive layer. The results from this model have been confirmed by 1D modelling.
- Hydrocarbon reservoirs may be identified by small anomalies, but only when the background model is known, and only for large reservoirs.

In summary, the EM response seem fairly little sensitive to variations in the model properties for the volcanics. However, in combination with other methods and applying sophisticated processing/inversion, SBL may still provide essential information for the solution of the basalt problem.

The EM results can be improved through advanced processing, like CMP- (1D inversion on CMP gathered receiver data) or 3D inversion. However, these methods should always be carried out in conjunction with 3D modelling and standard processed data analysis.

4. MT MODELLING

Grunde Waag, EMGS Oslo

4.1 Introduction

A MMT (Marine Magneto-Telluric) feasibility study was performed to assess the usefulness of MMT-data in a basalt setting.

The feasibility was assessed by first doing 2D forward modelling and then 2D inversion of the modelled response. 5% Gaussian noise was added to the response to make it more similar to a real acquisition situation. The inversion algorithm (*Occam inversion*, see de Groot-Hedlin and Constable (1990)) is based on a least structure approach by minimizing data misfit and model roughness. Both the TE- and TM-mode is inverted at the same time.

Two models were used in this study. The models were based on the surfaces shown in Figure *4.1*. The first model presented in Section 4.2, is a simple basalt model. It consists of the seafloor and the basalt structure.

The second model, presented in Section 4.3, includes the seafloor, the basalts, the Tertiary/Cretaceous boundary and the basement. The thin high resistive sill structures and reservoirs were assumed to have negligible effect on the response.

Frequencies from 0.5 mHz to 10 Hz were chosen for both models. The available frequencies in recorded data depend on the MMT-signal during the acquisition and the water depth. The seawater acts as a low-pass filter and attenuates the higher frequencies. 10 Hz is therefore an optimistic choice, but excluding the higher frequencies will not influence the result considerably.

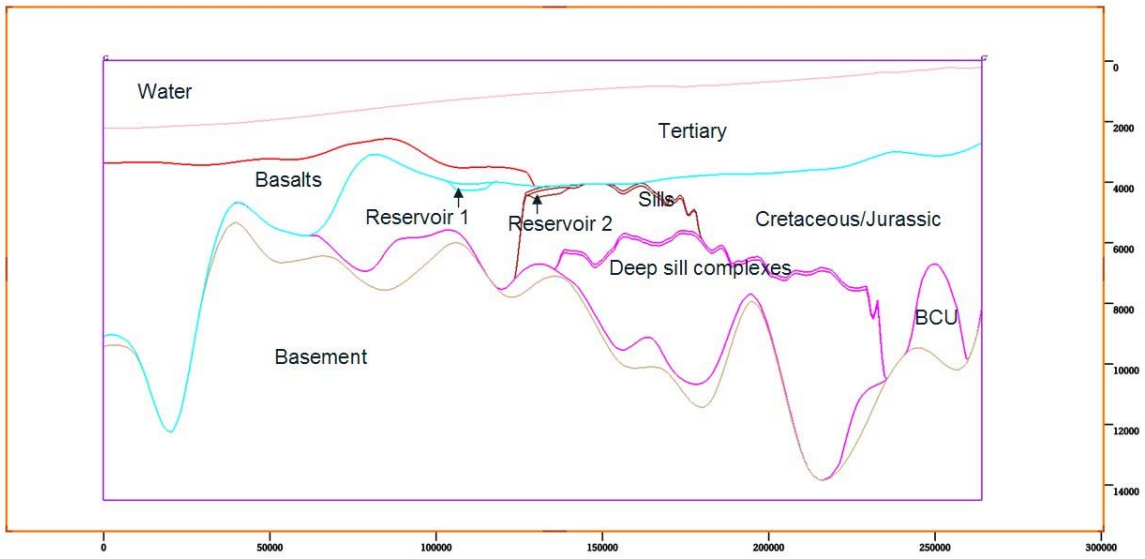

Figure 4.1 *Cross section of the model input. The seafloor, basalt layer and the basement were included in the 2D MMT-models.*

4.2 Simple basalt model

Seven receivers were placed on the sea floor above the basalt structure in this model, as seen in Figure 4.2. Four of the receivers were placed on top of the structure and three receivers were placed to the east of the basalt. The receiver spacing was 2 km and frequencies were chosen from 0.5 mHz up to 10 Hz.

The resulting model after six iterations is shown in Figure 4.3. There is no sign of the initial 100 Ωm basalt structure. The only structure seen in the inversion result is due to the 5% Gaussian noise added to the forward response.

The sensitivity to the basalt layer was tested by increasing the resistivity of the layer. When the basalt resistivity was increased to 5000 Ωm, the basalt started to be visible in the inversion results.

The apparent resistivity and phase modelled for receiver 002 and 007 are shown in Figure 4.4 and Figure 4.5. Receiver 002, which is located above the basalt, does not show a significant increase in apparent resistivity compared to receiver 007 which is located to the east of the basalt. Observations from forward modelling support the results from the inversion.

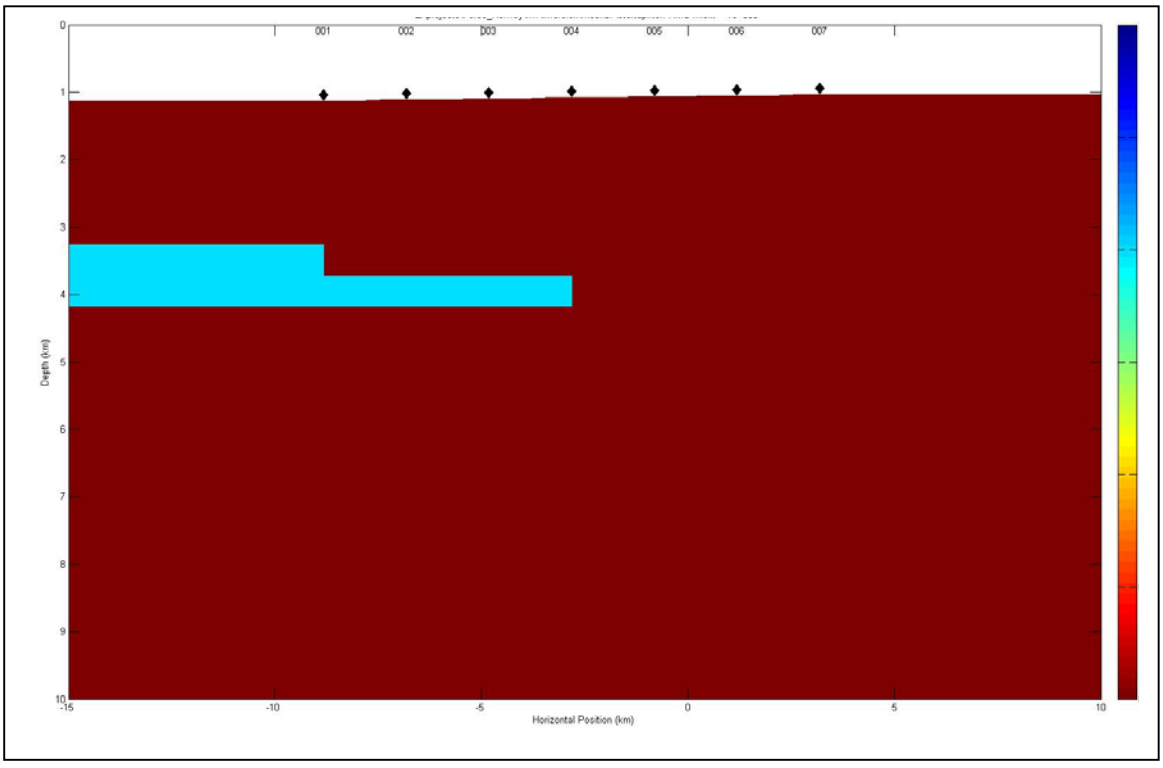

Figure 4.2 Model with only the basalt layer

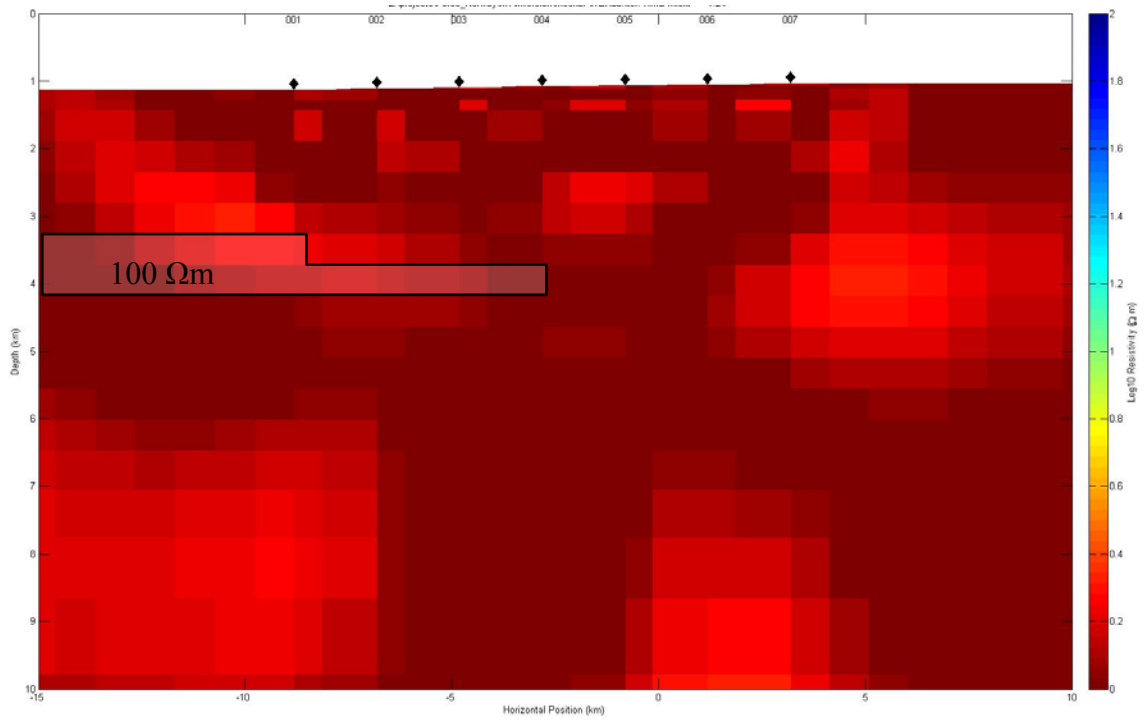

Figure 4.3 *Inversion result after the sixth iteration. Both the TE- and TM-mode is inverted at the same time.*

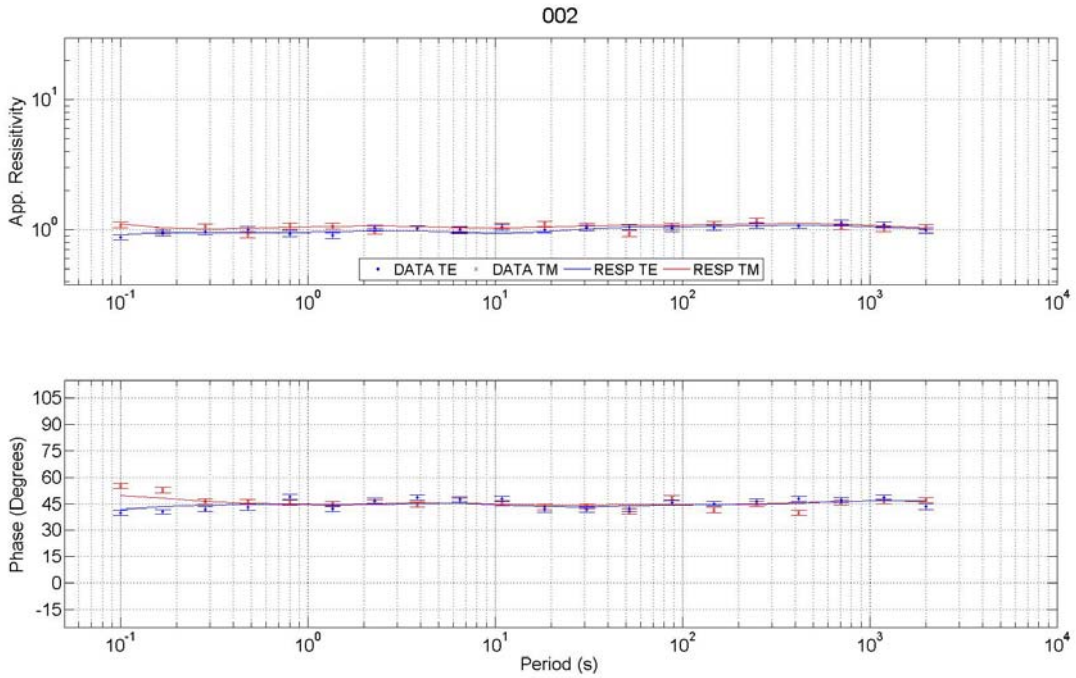

Figure 4.4 *Apparent resistivity and phase modelled for receiver 002 located on the seafloor above the basalt. The dots with error bars show the response from the forward modelling and the lines shows the response from the model obtained from inversion. Blue indicates transverse electric mode and red transverse magnetic.*

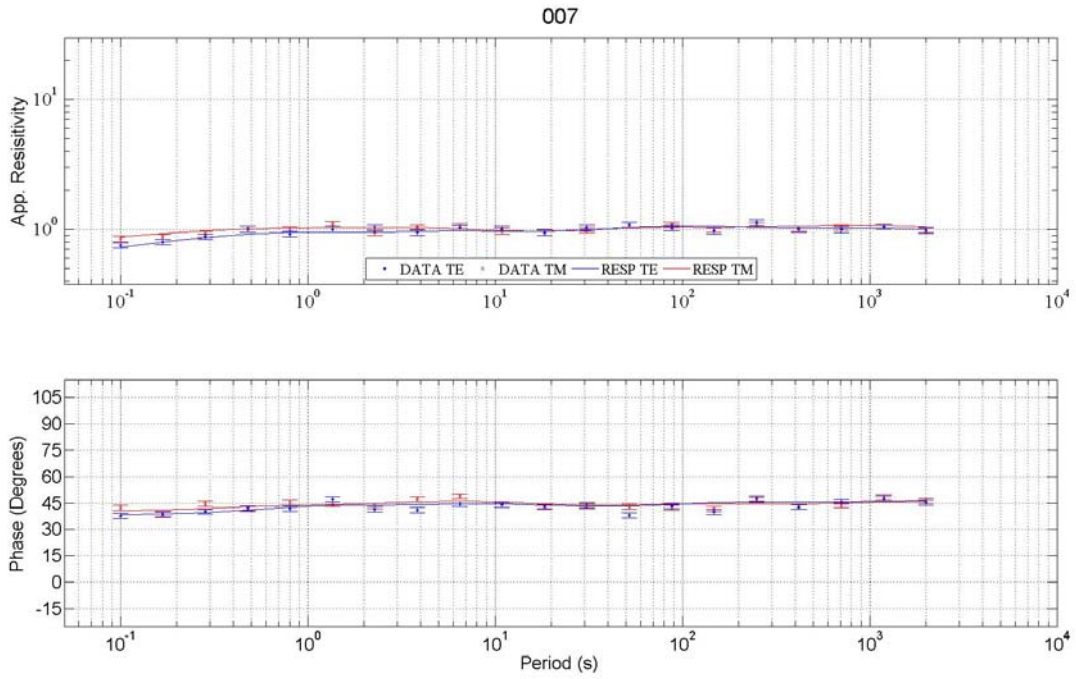

Figure 4.5 *Apparent resistivity and phase modelled for receiver 007 located on the seafloor to the east of the basalt. The dots with error bars show the response from the forward modelling and the lines shows the response from the model obtained from inversion. Blue indicates transverse electric mode and red transverse magnetic.*

4.3 Basalt and basement model

The second model used in this feasibility study included the basalt structure (100 Ωm) and the basement (50 Ωm). The starting model is shown in Figure 4.6. Twenty receivers with 5 km spacing were modelled using frequencies from 0.3 mHz to 10 Hz.

After four iterations the boundary of the basement is shown clearly (Figure 4.7). The basalt is not picked up by the inversion, as expected from the model shown in Section 4.2.

The response from receiver 002 and 017 is shown in Figure 4.8 and Figure 4.9. Receiver 002 is located on top of the most shallow part of the basalt and should therefore have an increased apparent resistivity at a higher frequency (shorter period) than receiver 017, which is located above a part of the basement which is about 3 km deeper. This clearly supports the inversion results shown in Figure 4.7.

A final model with a thicker basalt layer (100 Ωm) was tested. The starting model is shown in Figure 4.10. The basalt layer was increased in thickness from 500m to 1500m. The inversion result (12^{th} iteration) is shown in Figure 4.11. The response from receivers 002 and -017 is presented in Figure 4.12 and Figure 4.13, respectively. The basement is still visible in the inversion results, but now the basalt layer is also visible. However, the top of the basalt is not perfectly imaged, and the basement below the basalt is obscured by the presence of thicker basalt, obviously due to the thinned conductive sediment package. Where the sediment package is 3 km thick below the basalt, it is visible, where it is 1.5 km thick, it is not.

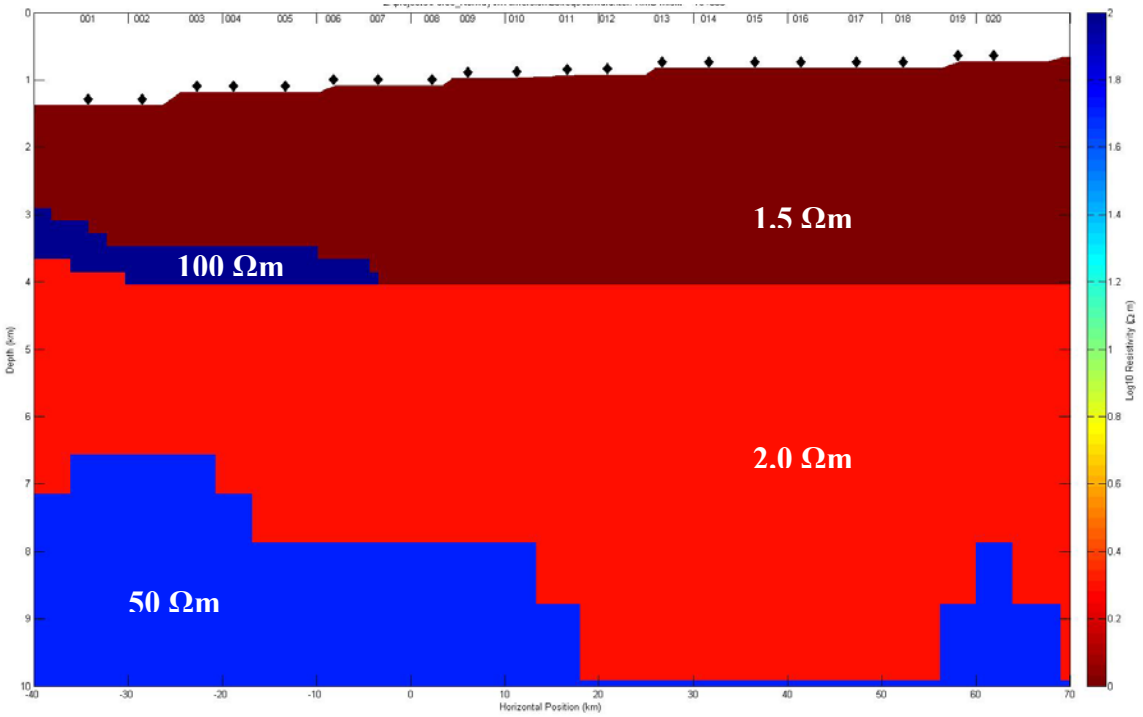

Figure 4.6 *Starting model including the basalt layer and the basement.*

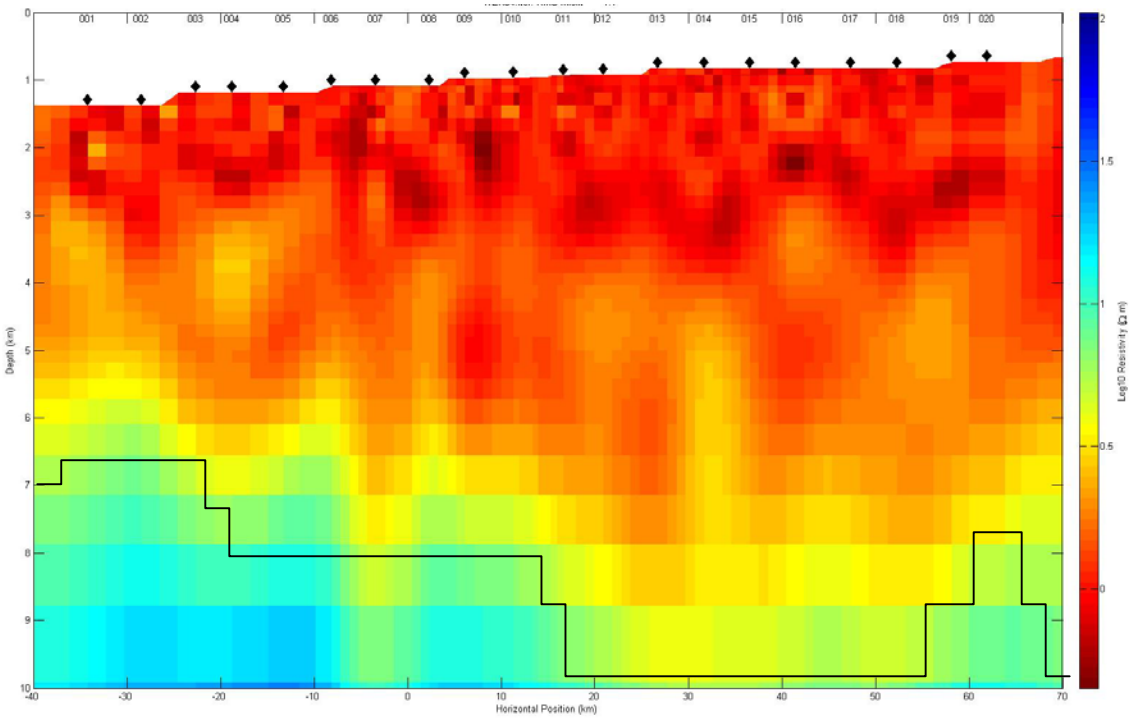

Figure 4.7 *Inversion results after the fourth iteration. The basement is clearly visible, but the basalt layer is not visible (as expected). The black curve indicates the basement boundary in the starting model.*

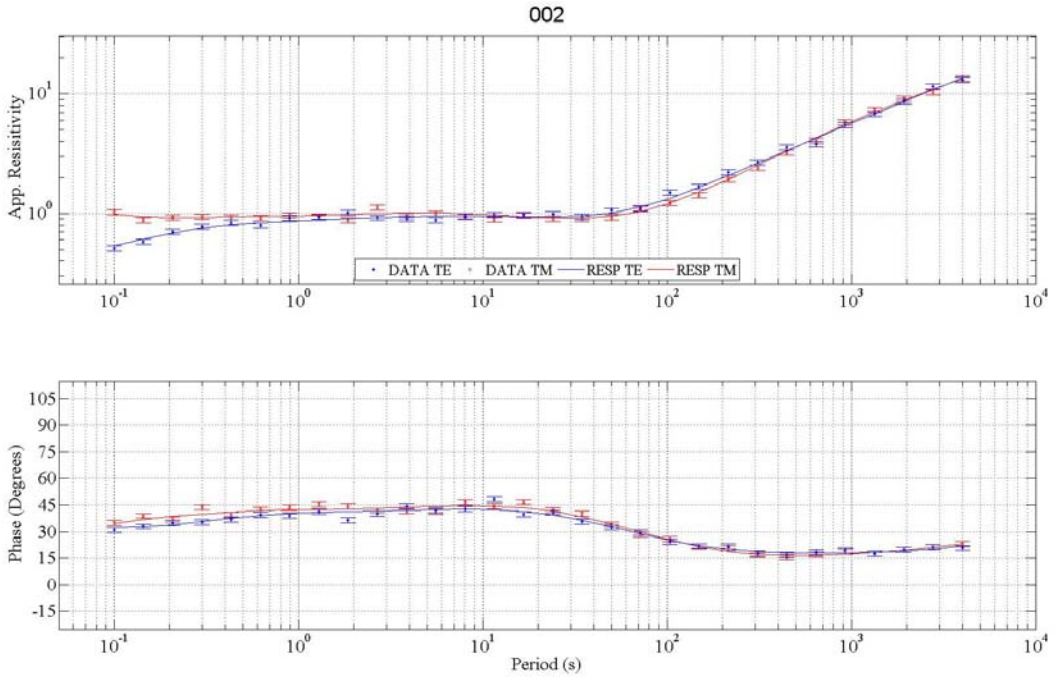

Figure 4.8 *Apparent resistivity and phase measured by receiver 002 located above the basalt. The dots with error bars show the response from the forward modelling and the lines shows the response from the model obtained from inversion. Blue indicates transverse electric mode and red transverse magnetic.*

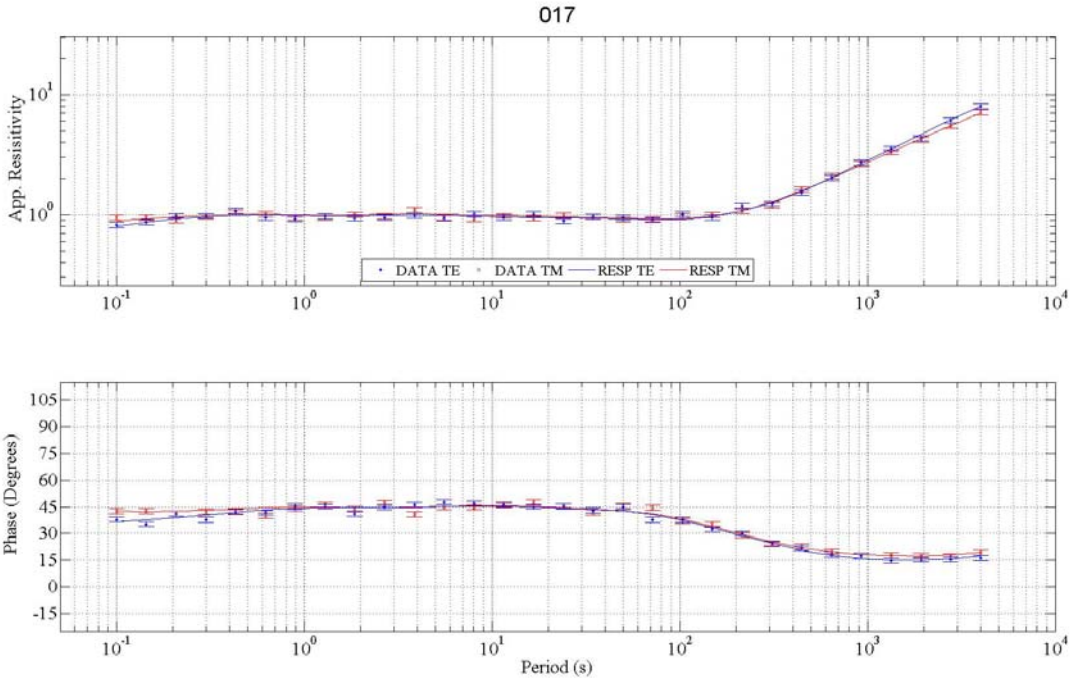

Figure 4.9 *Apparent resistivity and phase measured by receiver 017 located to the east of the basalt. The dots with error bars show the response from the forward modelling and the lines shows the response from the model obtained from inversion. Blue indicates transverse electric mode and red transverse magnetic.*

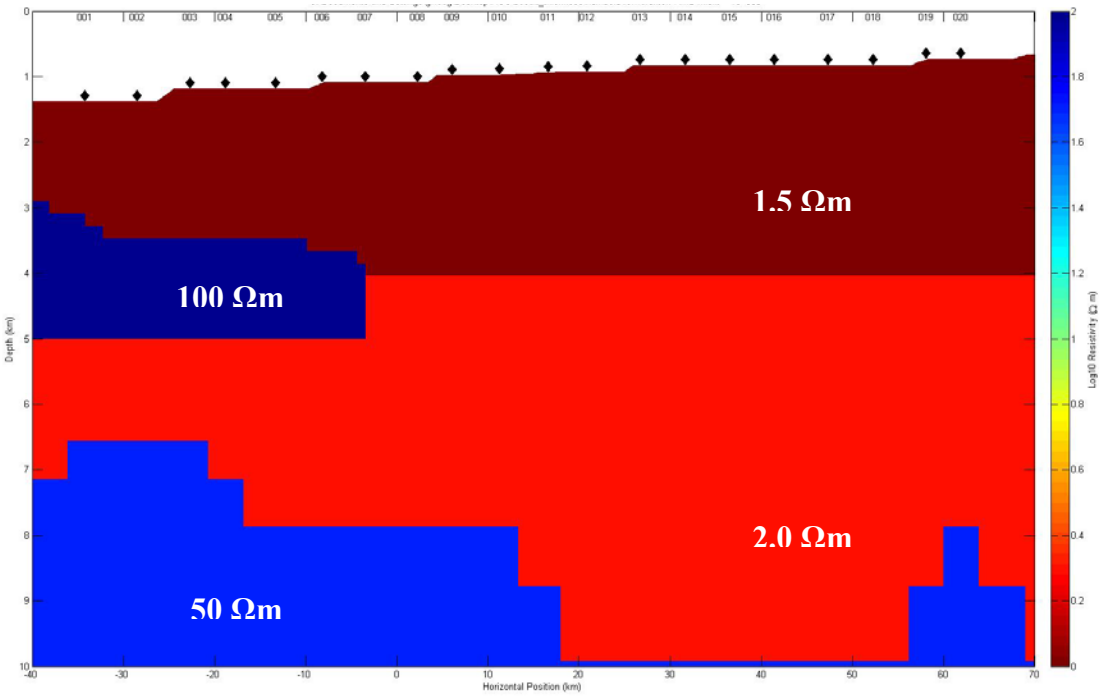

Figure 4.10 *Starting model including the basalt layer and the basement.*

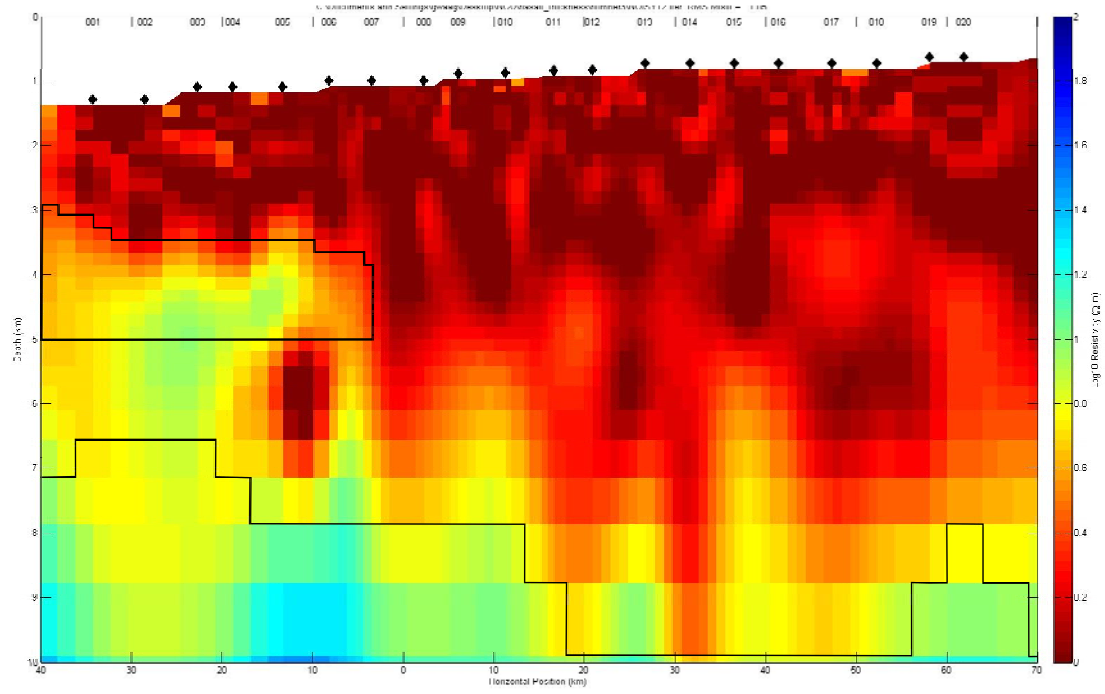

Figure 4.11 *Inversion results after 12th iteration. The basement is still visible in the inversion results, but now the basalt layer is also visible. However, the top of the basalt is not perfectly imaged, and the basement below the basalt is obscured by the presence of thicker basalt, obviously due to the thinned conductive sediment package. Where the sediment package is 3 km thick below the basalt, it is visible, where it is 1.5 km thick, it is not. The black curve indicates the basement and basalt boundaries in the initial model.*

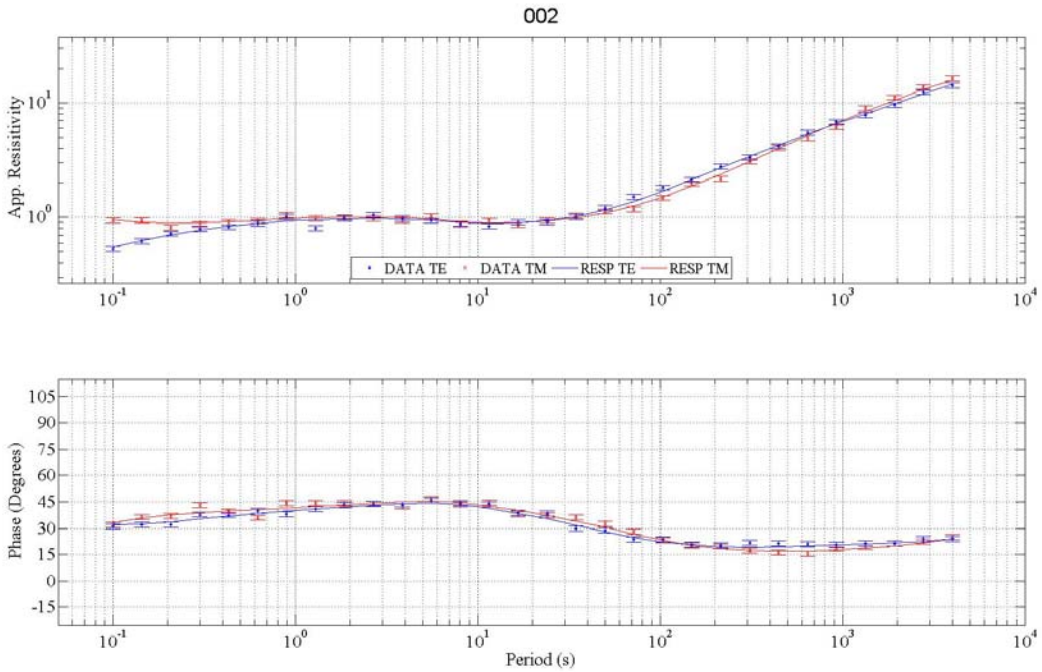

Figure 4.12 *Apparent resistivity and phase measured by receiver 002 located above the basalt. The dots with error bars show the response from the forward modelling and the lines shows the response from the model obtained from inversion. Blue indicates transverse electric mode and red transverse magnetic.*

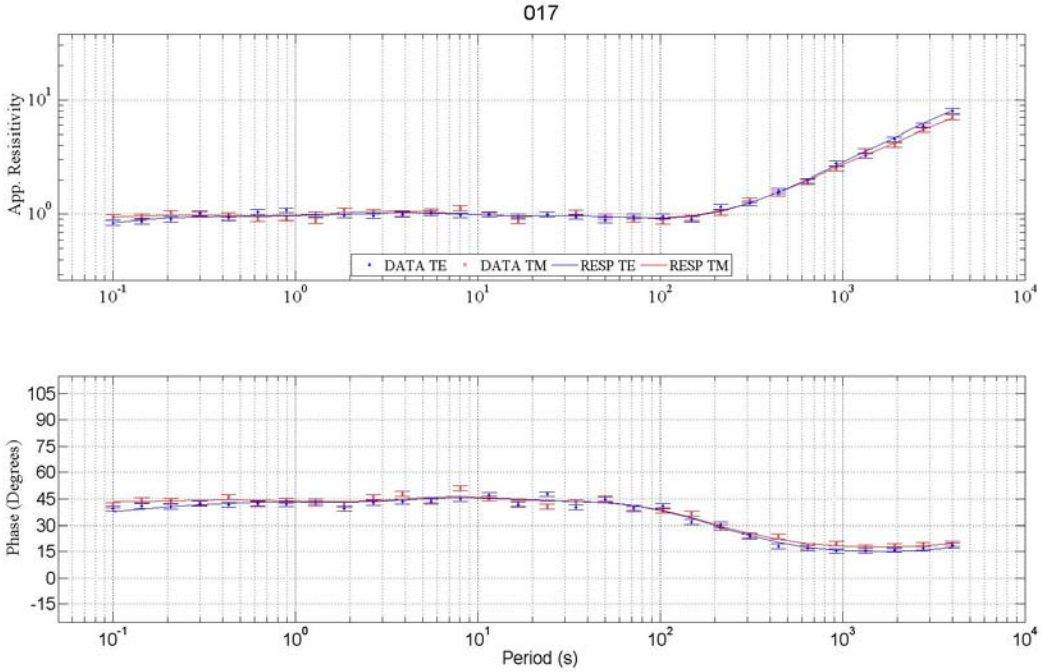

Figure 4.13 *Apparent resistivity and phase measured by receiver 017 located to the east of the basalt. The dots with error bars show the response from the forward modelling and the lines shows the response from the model obtained from inversion. Blue indicates transverse electric mode and red transverse magnetic.*

4.4 Summary of MMT results

2D inversion of two synthetic models was done in this feasibility study.

The models were simplified compared to the model used in the SBL model. Sills and reservoirs were not included in the 2D MMT models.

One model included only a simple basalt structure (100 Ωm). The MMT response was not sensitive to this structure, because the contrast to the background resistivity was too small. When the resistivity was increased to 5000 Ωm it started to appear in the inversion results (not shown in this report).

In the second model the basement was added, in addition to the basalt. The basement boundary can be seen clearly from the inversion results and in the individual receiver responses.

Finally, an increase in the basalt thickness was tested. The MMT results are now sensitive to the basalt layer, but fail to resolve the sediments between the basalts and the basement where the thickness is at its thinnest (1500 m).

5. SUMMARY AND CONCLUSIONS

Numerous experiments have demonstrated previously that standard seismic acquisition and processing techniques are not capable of characterizing volcanics or imaging beneath it. This study focused on the use of the potential fields in the sub-basalt imaging problem. Firstly, a 3D crustal model of the Møre Margin was constructed based on the gravity and magnetic fields. The modelling process was constrained by seismic interpretation, well studies and published physical properties. Secondly, several horizons from the resulting model were used as input for a 3D resistivity model. This model was then used to test the EM response in three different layouts. The results indicate little sensitivity of the EM method to varying volcanic properties. Thirdly, the feasibility of the MMT was assessed by a 2D forward modelling and inversion of the modelled response. Two geometrically distinct models with varying frequencies were constructed. The results demonstrate that the broad basement structure below the basalts can be identified from the MMT response.

The different geophysical methods applied in this study were:

- Seismic interpretation: sensitive to changes in acoustic impedance. Basalts have been shown to vary greatly internally and cause various disturbing effects in the seismic signal, e.g. attenuation and scattering. Nevertheless gives seismic reflection interpretation valuable geometrical constraint on top of flows and intrusions in volcanic basin settings. Recent developments in processing have also increased the quality of seismics in sub-basaltic environment.
- Gravity modelling: reflects density contrasts. In volcanic settings the greatest contrast is between the volcanics and sedimentary rocks on the one hand and the sedimentary rocks and basement on the other hand. As the bulk density parameter for the different bodies in the model can not be accurately defined, this method needs to be constrained by integration with other methods.
- Magnetic modelling: sensitive to variations in magnetic properties (i.e. susceptibility and remanence). The method is best suited to delineate the aerial extent of sills and lava flows. The thickness of sills and volcanic flows may be estimated if the magnetic properties are determined, e.g. from remanence measurements on core samples and from susceptibility logs. In conjunction with gravity modelling the method provides a valuable tool for basement recognition in not too severe basaltic settings.
- EM (SBL) measurements: sensitive to thin resistors. Apparently less sensitive to thickness increase of already very thick resistors.
- MMT: sensitive to conductors. In this context it can be used for detecting the base of sediments (= Top (resistive) Basement).

The work carried out in this study has demonstrated that no single method is capable of accurately defining the sub-basaltic structures. Each method detects different property contrasts to a varying degree. The integrated use of gravity, magnetics and seismic data give an indication of the broad sub-basaltic structures. Future work should focus on further

integration by accompanying the EM and MMT methods to the gravity and magnetic methods companied by seismic interpretations.

The gravity and magnetic compilations used in this study did not include all existing surveys in the area as they are non-released industrial data. A recent magnetic survey (NB-07) would increase the quality of the magnetic data compilation in the oceanward part of the study area. A more dense dataset could then be used to construct a more localized model that would decrease the geometrical uncertainty of the modelled bodies.

The great water depth (2-3 km) in the study area is a general problem when interpreting details from the potential field data. Perhaps a more appropriate study area would be the Vøring margin with shallower water depths and more data coverage.

Acquisition of gravity gradients are also of future interest in order to better resolve the sub-basaltic structures. Although fundamentally gravity gradient data contains no more information than conventional gravity data they are of interest from a practical point of view. Firstly, the horizontal resolution is about an order of magnitude better. Secondly, the gradient field falls off with distance as R^{-3} opposed to R^{-2} for gravity and hence is more sensitive to structures at shallow depths and therefore provides tighter constraints on the overburden structures. Thirdly, the gradients are useful in identifying linear structures indicative of horizontal lithology contrasts.

The integration of gravity data in seismic processing should also be a future task. Because of the better signal-to-noise ratio in gravity gradient data it can provide valuable input in velocity-depth models required in pre-stack depth migration (c.f. Smit et al. 2005). This could improve the quality of seismic in sub-basaltic settings that in turn would increase the constraints on the potential field methods.

6. PROPOSAL FOR FURTHER WORK

Peter Walker, Geophysical Algorithms, Mississauga, Ontario, Canada

The fundamental petroleum resource objective for this stage of the research is to understand how to define the thickness and depth of the basalt layers, and in particular, to understand how accurately these parameters can be determined. The ultimate objective is to develop a methodology to map basalt thicknesses and depths.

The approach taken to attack this problem is to use a blend of non-seismic, mainly potential field and electromagnetic, methods to define the stratigraphy of the basalts. The problem now being faced is that the resistivity and the thickness of the basalts are difficult to resolve, and a major objective of the next phase of the research is to develop an understanding and method of how this could be achieved. Electromagnetic studies to date, using a) magnetotelluric models and inversions and b) marine controlled source electromagnetic models and inversions have not been able to accomplish this goal. Potential field studies have indicated that the sediments are thick, and the potential for petroleum accumulation is large. However, the potential field data to not provide sufficient constraints on the properties of the basalt flows.

The most likely candidate for resolving the properties of the basalt flows are electromagnetic techniques. There is considerable potential for developing the electromagnetic method for this problem, building out from the preparatory work that has been done to date. Currently, it appears to be possible to derive some constraints on the resistivity-thickness product of the basalts, but the precise bound on this parameter is unclear. A major objective of the next phase of the research is to learn how to constrain the resistivity of the basalts, so that their thickness can be resolved separately as a distinct parameter.

This proposal is directed towards the goal of improving our understanding to better defining the depth and thickness of the basalts, and the factors that contribute to any errors or uncertainties in the thickness estimates. With billions of dollars of oil potentially in play, this problem should be solvable. New survey technology may be required.

6.1 Governing Physical Principles

The scope of work in this proposal is based on the following physical principles governing electromagnetic interpretation:

The effect of the air-water interface distorts EM measurements and must be understood to properly map sub-sea rock parameters.
Marine CSEM data is dominantly sensitive to the resistivity-thickness product of a resistive layer when the layer is deep and thin relative to the dimensions of the survey apparatus.

The thickness of a resistive layer can be better resolved from a marine CSEM source if the layer resistivity is known.

Inductive sources (for example, MT) can be used to define the conductivity-thickness products of layers. Where the skin depth is comparable or smaller than the thickness of the layer, the conductivity and the thickness of the layer can be resolved separately.
Seismic data may provide an accurate estimate to the top of the basalt layers, further improving the quality of the resistance and thickness parameters obtained from the electromagnetic data.

Inductive sources, when the right frequencies are used, can resolve the conductivity and thickness of the sediments overlying the basalts, so as to provide information on the depth of the basalts. Together with constraints on top-of-basalt from seismic data, it should be possible to resolve the conductivity of the overlying sediments.
Certain CSEM layouts may also be useful in characterizing the sediments over the basalts.

By accurately mapping the sediments over the basalts, the character (resistivity and thickness) of the basalts can be more accurately parameterized.

Ocean bottom MT excitation may not have sufficient energy in the required frequency bands to resolve the conductivity and thickness of the sediments over and directly under the basalts. A new source of inductive energy may be required.

CSEM layouts (scales, offsets and frequencies) may have to be adjusted to better resolve the required parameters.

Data from inductive sources (for example MT, or a new system to be developed), and galvanic sources (for example marine CSEM) provide complementary data sets that, when used together, improve the resolution of both conductive and resistive layers.

These principles can be applied to the problem of resolving the depth and thickness of sub-sea basalt layers as follows:

In the western part of the survey area, the basalts may be thick enough relative to their depth that a CSEM survey may be able to distinguish their resistivity and thickness as separable parameters

Eastward from the western area where the basalts are shallow, the resistivity information measured from the western basalts can be used to constrain the resistivity of the eastern extension of these basalts, and so improve thickness-estimates of the deeper basalts where the resistivity and thickness parameters would otherwise not be separable.
Deeper basalts will be best resolved using different frequencies and scales than used to resolve the shallow basalts.

Magnetotelluric or other inductive source data may constrain the conductivity and thickness of the sediments overlying the basalts, provided energy exists in the necessary frequency bands.

Inductive source energy will energize currents in the sediments below the basalts, so assisting the CSEM data in resolving the thickness of the basalt layers.
Uncertainly in the properties of the basalts (thickness and resistivity) will be reduced by accurately mapping the electrical properties of the overlying sediments.

6.2 Proposed Scope of Work

The scope of work proposed below is a step-by-step approach to understanding how to determine the thickness and depth to the basalts. It is based on the principles outlined in the previous section. One complicating factor is the effect of the air-water interface, which complicates understanding the secondary field response of the sediments.

1. Air/ocean interface effects:
A problem that complicates the interpretation of the sea-bottom CSEM data is the reflection of energy from the impedance contrast at the air-ocean interface. It should be possible to eliminate this effect and some modeling will be done to understand how this might be done. One problem with conventional up-down separation is that it may contain residual errors that have magnitudes on the order of the signals from the targeted basalts, complicating the resolution of those bodies.

2. Basalt resistance – CSEM sounding:
If the thickness of the basalts is to be known, and because the thickness of the basalts is not large relative to their depth, their thickness must be separated from a more important parameter, the resistivity-thickness product. Accordingly, the resistivity of the basalts must first be known.

We propose to model the basalts in the western part of the study area where they appear to be thick enough in comparison to their depth to develop an understanding of their resistivity. By setting up the model as a sounding problem, and resolving the thickness and conductivity of the overlying sediments first, it may be possible by clever use of sensor arrays to be able to extract their resistivity and so resolve their thickness. Part of this work would be to understand how to remove the uncertainly of the resistance of the overlying sediments. In doing so, the resistance of the basalts should be better constrained. This work would be done with a 1-dimensional model.

3. MT data – review of applicability:

The MT data are likely to provide limited information on the basalts themselves, because the MT data would tend to be more sensitive to conductive layers. However, the MT data may be useful for defining the conductivity and thickness of the sediments sandwiching the basalts. One problem with the MT data may be that the energy in the high-frequency signals may be too small to be useful in resolving the conductivity and thickness of those sediments (The periods used by EMGS were 0.1 sec - 20 minutes, which could be too large to properly resolve the near surface layers of the sediments.) The MT data will be modelled to determine the frequency bands that are required to provide information to constrain the conductivity and the thickness of those sediments. It might be possible to construct a virtual inductive source using CSEM data to complement the MT data in the high frequencies.

4. Joint use of galvanic and inductive data:

It is known that galvanic source data and inductive source data provide complementary sounding information, the first being sensitive to the resistivity-thickness of a layer, the second being sensitive to the conductivity-thickness. Depending on the assessment of the MT data, it may be possible to improve the resolution of the sediment and basalt layer conductivities and thicknesses using both data sets together.

5. Other CSEM configurations:

It is probable that the joint use of inductive and galvanic excitation will improve the resolution of the basalts. If the MT data prove to be ineffective in resolving the sediments over, and directly under, the basalts, then some modeling will be done to investigate the potential of using alternate methods to energize the sea bottom so as to resolve the basalts. The most likely candidates would be a) a large coil transmitter that could be towed over the sea bottom from a surface ship, using sea-bottom magnetometers as receivers, or b) a coil that could be dropped to the sea bottom with roving submersables used to measure the magnetic field in profiles, or c) a combination of towed coil and roving submersables. The coil transmitter would complement the energization from the CSEM configuration now deployed. It may be possible to construct a virtual coil transmitter from conventional CSEM data. All the configurations suggested have analogues to EM systems deployed in mining geophysics.

6. Evaluation of the thickness of deeper basalts:

If the resistance of the basalts can be constrained using the methods of 2 or 5 above, then we propose to evaluate how well the thickness of the thicker basalt layer can be resolved where it appears to become deeper towards the centre of the study area. The approach here would be to constrain the resistance of the basalts and compute the resulting uncertainties in thickness for various depths.

7. REFERENCES

Abrahamsen, N., Schoenharting, G. & Heinesen, M. 1984. Palaeomagnetism of the Vestmanna core and magnetic age and evolution of the Faeroe Islands. In: *The deep drilling project 1980-1981 in the Faeroe Islands* (edited by Berthelsen, O., Noe-Nygaard, A. & Rasmussen, J.). Føroya Fróðskaparfelag, Tórshavn, 93-108.

Abrahamsen, N. & Waagstein, R. 2006. Magnetic logs from the Lopra-1/1A and Vestmanna-1 wells, Faroe Islands. *Geological Survey of Denmark and Greenland Bulletin* **9**, 41-49.

Andersen, O. B. & Knudsen, P. 1998. Gravity anomalies derived from the ERS-1 satellite altimetry. Kort og Martykelstyrelsen, Copenhagen.

Balling, N., Kristiansen, J. I. & Saxov, S. 1984. Geothermal measurements from the Vestmanna-1 and Lopra-1 boreholes. In: *The deep drilling project 1980-1981 in the Faeroe Islands* (edited by Berthelsen, O., Noe-Nygaard, A. & Rasmussen, J.). Føroya Fróðskaparfelag, Tórshavn, 137-147.

Breivik, A., Mjelde, R., Faleide, J. I. & Murai, Y. 2006. Rates of continental breakup magmatism and seafloor spreading in the Norway Basin–Iceland plume interaction. *Journal of Geophysical Research* **111**(B07102).

Breivik, A., Verhoef, J. & Faleide, J. I. 1999. Effect of thermal contrasts on gravity modeling at passive margins: Results from the western Barents Sea. *Journal of Geophysical Research* **107**(B7), 15293-15311.

De Groot-Hedlin, C. and Constable, S.C., 1990: "Occam's inversion to generate smooth, two dimensional models from magnetotelluric data". *Geophysics* **55**, p1613-1624.

Dehls, J. F., Olesen, O., Bungum, H., Hicks, E., Lindholm, C. D. & Riis, F. 2000. Neotectonic Map, Norway and Adjacent Areas (1:3 milljon). Geological Survey of Norway, Trondheim.

Dziewonski, A. M. & Anderson, D. L. 1981. Preliminary Reference Earth Model. *Physics of the Earth and Planetary Interiors* **25**(4), 297-356.

Ebbing, J., Lundin, E., Olesen, O. & Hansen, E. K. 2006. The mid-Norwegian margin; a discussion of crustal lineaments, mafic intrusions, and remnants of the Caledonian root by 3D density modelling and structural interpretation. *Journal of the Geological Society* **163**(1), 47-59.

Eldholm, O. & Mutter, J. C. 1986. Basin structure on the norwegian margin from analysis of digitally recorded sonobuoys. *Journal of Geophysical Research* **91**(B3), 3763-3783.

Eldholm, O., Thiede, J. & Taylor, E. 1987. Proceeding Oceanic Drilling Program, Initial Reports 104, College Station, TX (Ocean Drilling Program).

Fernàndez, M., Ayala, C., Torne, M., Verges, J., Gomez, M. & Karpuz, R. 2005. Lithospheric structure of the mid-Norwegian margin; comparison between the More and Voring margins. *Journal of the Geological Society* **162**(6), 1005-1012.

Fernàndez, M., Torne, M., Garcia-Castellanos, D., Vergés, J., Wheeler, W. & Karpuz, R. 2004. Deep structure of the Vøring Margin: the transition from a continental shield to a young oceanic lithosphere. *Earth and Planetary Science Letters* **221**(1-4), 131-144.

Franzson, H., Guðlaugsson, S. & Friðleifsson, G. Ó. 2001. Petrophysical Properties of Icelandic Rocks. In: *6th Nordic Symposium on Petrophysics*, Trondheim, Norway, 1-14.

Friðleifsson, I. B. 1982. The Iceland Research Drilling Project in relation to the geology of Iceland. *Journal of Geophysical Research* **87**(B8), 6363-6370.

Friðleifsson, I. B., Gibson, I. L., Hall, J. M., Johnson, H. P., Christensen, N. I., Schmincke, H.-U. & Schönharting, G. 1982. The Iceland Research Drilling Project. *Journal of Geophysical Research* **87**(B8), 6359-6361.

Helgason, J. 1982. Magnetostratigraphy of the exposed lava section east of the IRDP drill hole in Reydarfjordur, Eastern Iceland. *Journal of Geophysical Research* **87**(B8), 6396-6404.

Jónsson, G. & Stefánsson, V. 1982. Density and porosity logging in the IRDP hole, Iceland. *Journal of Geophysical Research* **87**(B8), 6619-6630.

Kent, D. V. & Opdyke, N. D. 1978. Paleomagnetism and magnetic properties of igneous rock samples - Leg 38. In: *Initial Reports of the Deep Sea Drilling Project, Supplements to Vol. 38, 39, 40 and 41* (edited by Talwani, M., Udintsev, G. & White, S. M.). U.S. Government Printing Office, Washington.

Kinck, J. J., Husebye, E. S. & Larsson, F. R. 1993. The Moho Depth Distribution in Fennoscandia and the Regional Tectonic Evolution from Archean to Permian Times. *Precambrian Research* **64**(1-4), 23-51.

Kristjansson, L. & Helgason, J. 1988. Some properties of basalt lava sequences and volcanic centres in a plate-boundary environment.; Early Tertiary volcanism and the opening of the NE Atlantic. *Geological Society Special Publications* **39**, 147-155.

Laxon, S. & McAdoo, D. 1994. Arctic Ocean Gravity Field Derived From ERS-1 Satellite Altimetry. *Science* **265**.

Mørk, M. B. E., McEnroe, S. A. & Olesen, O. 2002. Magnetic susceptibility of Mesozoic and Cenozoic sediments off Mid Norway and the role of siderite: implications for interpretation of high-resolution aeromagnetic anomalies. *Marine and Petroleum Geology* **19**(9), 1115-1126.

Olesen, O., Gellein, J., Håbrekke, H., Kihle, O., Skilbrei, J.R. and Smethurst, M.A. 1997. Magnetic anomaly map, Norway and adjacent ocean areas. Scale 1:3 million. Geological Survey of Norway.

Olesen, O., Lundin, E., Nordgulen, O., Osmundsen, P. T., Skilbrei, J. R., Smethurst, M. A., Solli, A., Bugge, T. & Fichler, C. 2002. Bridging the gap between the onshore and offshore geology in Nordland, northern Norway. *Norwegian Journal of Geology* **82**(4), 243-262.

Ólafsson, I., Sundvor, E., Eldholm, O. & Grue, K. 1992. More Margin - Crustal Structure from Analysis of Expanded Spread Profiles. *Marine Geophysical Researches* **14**(2), 137-162.

Pálsson, S., Haraldsson, G. I. & Vigfússon, G. H. 1984. Eðlismassi og poruhluti bergs. Orkustofnun, Reykjavík, 35.

Planke, S. & Alvestad, E. 1999. Seismic volcanostratigraphy of the extrusive breakup complexes in the northeast Atlantic: implications from ODP/DSDP drilling. *Proceedings of the Ocean Drilling Program, Scientific Results* **163**, 3-16.

Planke, S., Cerney, B., Bücker, C. J. & Nilsen, O. 1999. Alteration effects on petrophysical properties of subaerial flood basalts: Site 990, southeast Greenland margin. *Proceedings of the Ocean Drilling Program, Scientific Results* **163**, 17-28.

Planke, S. & Eldholm, O. 1994. Seismic Response and Construction of Seaward Dipping Wedges of Flood Basalts - Voring Volcanic Margin. *Journal of Geophysical Research-Solid Earth* **99**(B5), 9263-9278.

Planke, S., Skogseid, J. & Eldholm, O. 1991. Crustal structure off Norway, 62° to 70° north. *Tectonophysics* **189**(1-4), 91-107.

Raum, T., Mjelde, R., Digranes, P., Shimamura, H., Shiobara, H., Kodaira, S., Haatvedt, G., Sorenes, N. & Thorbjornsen, T. 2002. Crustal structure of the southern part of the Voring Basin, mid-Norway margin, from wide-angle seismic and gravity data. *Tectonophysics* **355**(1-4), 99-126.

Raum, T., Mjelde, R., Shimamura, H., Murai, Y., Bråstein, E., Karpuz, R. M., Kravik, K. & Kolstø, H. J. 2006. Crustal structure and evolution of the southern Vøring Basin and Vøring Transfrom Margin, NE Atlantic. *Tectonophysics* **415**, 167-202.

Saxov, S. & Abrahamsen, N. 1964. A note on some gravity and density measurings in the Farow Islands. *Bollettino di Geofisica Teorica ed Applicata* **6**(23), 249-262.

Schoenharting, G. & Abrahamsen, N. 1984. Magnetic investigations on cores from the Lopra-1 drillhole, Faeroe Islands. In: *The deep drilling project 1980-1981 in the Faeroe Islands* (edited by Berthelsen, O., Noe-Nygaard, A. & Rasmussen, J.). Føroya Fróðskaparfelag, Tórshavn, 109-114.

Smit, D.-J., Biegert, E. & Mondt, J. 2005. Advances in subsurface imaging using potential field technology: gravimetry sensors and applications. In: *Petroleum Geology: North-West Europe and Global Perspectives - Proceedings of the 6th Petroleum Geology Conference* (edited by Doré, A. G. & Vining, B. A.). Geological Society, London, 1453-1459.

Telford, W. M., Geldart, L. P. & Sheriff, R. E. 1990. *Applied Geophysics*. Cambridge University Press, Cambridge.